Volcanic spherules condensed from supercritical fluid in the Payenia volcanic province, Argentina

Volcanic spherules condensed from supercritical fluid in the Payenia volcanic province, Argentina

Linda A. Kirstein[a]; Silvestar Kanev[a]; J. Godfrey Fitton[a]; Stephen J. Turner[b]; EIMF[c]

[a]School of GeoSciences, University of Edinburgh, Grant Institute, James Hutton Road, EH9 3FE, UK

[b]Washington University in St. Louis, One Brookings Drive, St. Louis, MO 63130, USA

[c]Edinburgh Ion Microprobe Facility, Grant Institute, University of Edinburgh, EH9 3FE, UK

Abstract: Spherules can be formed by high temperature processes during volcanic eruptions, lightning strikes and meteorite impacts. Here we report four different types of spherules and spheroidal particles associated with tephra deposits from two separate volcanic fields in the southern Payenia province of Argentina. These silicate and carbonate spherules represent <0.01 % of the sampled material with individual spherules <200 µm in size. Thirty particles have been imaged, only the transparent spherules are smooth, perfect spheres. Other morphologies include ellipsoids and aggregated dumbbells, and the spheroids are hollow or solid. Major-element analyses show that the spherules and spheroids have silica-rich, iron-rich, carbonate and basaltic compositions. Chemical analysis of the carbonate spheroids shows some variability in trace element content between the cores and rims suggesting element mobility and loss towards the margins. All analysed carbonate spheroids have elevated Sr/Y, La/Y and La/Ce, outside of the range of sedimentary carbonate. All four spherule types are considered volcanic in origin, with the excess CO_2 required for the formation of carbonate spherules potentially sourced from basement lithologies. Based on major- and trace-element analyses we conclude that the silica-rich and carbonate spherules formed by instantaneous condensation from supercritical CO_2-rich hydrous fluids saturated with dissolved silicates.

Key words: Volcanic spherules; tephra; supercritical fluids; eruption dynamics; silicate; carbonate; Payenia.

Supplementary material: Appendix A. Full electron and secondary ionisation microprobe dataset.

Spherules of varying compositions (e.g. silica-rich, Fe-rich) have been documented associated with different types of Earth and planetary processes, including cosmic spherules (Taylor and Brownlee 1991; Genge et al. 2017), volcanic eruptions (Macdonald et al. 1993; Meeker and Hinkley 1993; Obenholzner et al. 2003) and both volcanic and cloud-to-ground lightning strikes (Pasek et al. 2012; Genareau et al. 2015). Spherical particle morphologies are inconclusive in discerning origin as they can form naturally through biogenic, volcanogenic, diagenetic as well as extra-terrestrial or impact processes. The mechanism by which spherical particles form are well known, particularly the effects of nucleation, adsorption, condensation, coagulation, lightning, heating duration, and sintering. The size and composition of spherules produced naturally is highly variable depending on the mechanism of formation (Hodge and Wright 1964; Wright and Hodge 1965; Genareau et al. 2015; Genge et al. 2017; Suttle and Folco 2020). However, common to many non-biogenic processes is the need for high temperatures above the glass transition or solidus to melt the particle(s) and form spheres primarily under the action of surface tension (Wadsworth et al. 2017). The temperatures required for melting to take place can be achieved in three distinct ways: (i) high velocity impacts or flash heating during atmospheric entry of extra-terrestrial material; (ii) lightning strikes; and (iii) volcanic activity. Not all particles form perfect spherules; the more irregular shaped are termed spheroids (Wright et al. 1965). Here we summarise some of the formation mechanisms proposed in the literature and use these to provide a framework in an attempt to determine the origin of spherules and spheroidal particles detected in volcanic tephra from the Auca Mahuida and Tromen volcanic regions in the southern Payenia part of the Andes mountain range of South America (Figure 1). We find that none of the known mechanisms is capable of explaining a suite of perfect carbonate and high-silica glass spherules, and we propose that these formed by condensation from a hydrous supercritical fluid released during eruption.

Spherules related to bolide impact or flash-heating on atmospheric entry

Spherules associated with major bolide impact events have been described since the 1960s associated with Chicxulub ejecta (Mexico; Schulte et al. 2003), Acraman ejecta (South Australia; Wallace et al. 1990), Victoria Land (Antarctica; Folco et al. 2016), Barberton greenstone belt (South Africa; Ozdemir et al. 2017) and the Younger Dryas bombardment (Wu et al. 2013) amongst others. Depending on the angle at which extra-terrestrial

impactors hit the Earth's surface, a shock wave is generated that compresses the rock to very high pressures, some of the rock is vaporised and there is a substantial amount of melt generated. The ejecta are projected away from the impact site and include impact melt droplets of variable size and composition. Distal impact glasses include tektites and impact spherules which may or may not contain microlites (Glass 2016). Impact spherules form through condensation from the resultant impact plume, while tektites are produced by melting. Magnetic microspherules, carbon spherules, glassy spherules with relict minerals, Fe-rich glass, K-rich glass and compositionally mixed particles have all been described from impact craters (Graup 1999; Ohtaki et al. 2019).

Micrometeorites are formed by melting of extra-terrestrial dust during atmospheric entry, while ablation spherules are shed from the outer surfaces of larger meteorites during atmospheric entry (Genge et al. 2008). The degree of melting that a micrometeorite experiences is dependent on particle size, entry velocity and entry angle (Love and Brownlee 1991). Completely melted particles are termed cosmic spherules; they comprise 50 to >90% of the particles recovered in the size range from 50-100 µm and are olivine- and glass-dominated spheres (Genge et al. 2008; Suttle and Folco 2020). Chemical subtypes of cosmic spherules include iron-rich (I-type) and silicate (S-type) (Genge et al. 2008). Spheres composed of iron oxides (magnetite and wüstite) are also found but account for <5% in collections (Suttle and Folco 2020). These magnetic spherules were the focus of early work that tried to differentiate between meteoritic and volcanic spherules (Hodge and Wright 1964; Franklin et al. 1967). Cosmic spherules often have distinct surface textures including well-developed crystalline dendrites or regular polygonal textures of equant crystals (Mutch 1964). The spherules are highly variable in composition; magnetic I-type micrometeorites tend to have low Ti <0.5wt% and high Fe >70 wt.% (Voldman et al. 2013), and S-type cosmic spherules, which are the most common micrometeorite type, have chondritic compositions (Genge et al. 2008).

Lightning-induced spherules

Fulgurites are glasses formed from the fusion of rock by lightning (Essene and Fisher 1986; Pasek et al. 2012). During volcanic eruptions ash can induce volcanic lightning in the atmosphere which, due to the extreme temperatures (~30,000 K) during discharge, can result in localised melting of particles in the volcanic plume as documented for example at

Sakurajima volcano, Japan (Smith et al. 2018). Although the timescale for discharge is very short it is more than sufficient to melt fine (<63 µm) ash particles (Genareau et al. 2015), and modelling suggests that grains up to 150 µm can melt (Wadsworth et al. 2017).

There are morphological differences between cloud-to-ground fulgurites and lightning-induced volcanic spherules. Fulgurites tend to be tubular with irregular outer surfaces, varying in size from milimetres to metres (Essene and Fisher 1986; Pasek et al. 2012). Droplet fulgurites are known to occur, but more rarely, with diameters >1cm; their textures are consistent with ejection from a fulgurite cylinder and cooling on the ground (Pasek et al. 2012) which leads to sub-spherical forms. Droplet fulgurites tend to be more homogeneous in composition and are richer in SiO_2 and K_2O than other fulgurite types (Pasek et al. 2012).

The diameter of spherules created during current impulse experiments, performed to replicate volcanic lightning discharge, range from ~3 to 43 µm (Genareau et al. 2015; Genareau et al. 2019), with melting and degassing of ash aggregates forming variably shaped pumice fragments > 100 µm (Genareau et al. 2019). Hollow spheres of glass are formed as a result of bubble detachment from these degassing aggregates (Genareau et al. 2019). By comparison, volcanic spherules collected from natural eruptions (e.g. Mount Redoubt and Mount Pavlof, Alaska, USA; Eyjafjallajökull, Iceland), where volcanic lightning was documented, are larger (9-81 µm) and have either cracked or hollow forms (e.g. Genareau et al. 2015).

Particles produced during experiments can be vesiculated with smooth outer surfaces that form either spherical or teardrop shapes and occur either aggregated or in single form (Genareau et al. 2019). Expansion of structurally bound water has been proposed to explain their morphologies. Compositionally the particles are dominated by Si with lesser Al, K, Ca and Fe (Genareau et al. 2015). Spherules formed in flash-over experiments commonly have a flattened side where they have been bound to other particles, while fluidal morphologies dominate larger particles (Genareau et al. 2015). Ash-melting experiments using a lightning arc also show partial melting, rounding, foaming and particle fragmentation (Mueller et al. 2018). Loss of Cl, S, P and Na through vaporisation was measured post melting but morphologies were reported to be similar to natural examples (Mueller et al., 2018).

Carbonate spherules

Carbonate spherules can form through a wide range of geological processes, and determining whether they are primary (related to magma composition and eruption dynamics) or secondary (e.g. weathering related) in origin is difficult. Textural evidence supporting formation through liquid immiscibility might include carbonate globules within silicate glass, coalescing carbonate spheres, budding between silicate and carbonate melt and evidence of quench crystallisation (Graup 1999; Brooker and Kjarsgaard 2010). Carbonate globules are a feature of high temperature silicate-carbonate immiscibility melt experiments at 0.1 to 2.5 GPa with some deformation observed where smaller globules impinge on larger ones (Brooker and Kjarsgaard 2010). By contrast, fibrous growth or zoned calcite tends to suggest secondary formation.

Carbonate-silicate immiscibility has been shown to occur during impact melting at the Ries Crater (Germany) (Graup 1999) and also associated with the Chicxulub impact (Mexico; Schulte et al. 2003). At both impact sites the spherules are considered primary and result from melting of the pre-impact basement lithologies including chalk, marls and sandstones as well mafic and felsic igneous rocks (Graup 1999; Schulte et al. 2003). Primary ejecta included mixed melt and unmelted debris resulting in the impact melt-bearing breccia suevite (Graup 1999).

Finally carbonate formed in different geological environments has different chemical compositions. Magmatic calcite from Ca-carbonatites is remarkably enriched in some trace elements including Sr (>7800 ppm), Ba (>328 ppm) and rare earth elements (ΣREE >335 ppm) (Hornig-Kjarsgaard 1998). Carbonates from marine environments are much less enriched in trace elements (Sr: 610 ppm; Ba: 10 ppm) (Veizer 1983).

Volcanic spherules

Volcanic eruptions inject considerable quantities of fine particles of volcanic and non-volcanic origin as well as gases into the atmosphere. The term volcanic ash refers to particles < 2mm in size and the amount of ash generated depends on a variety of different factors including volatile content, viscosity, magma composition, rate of degassing and

151 eruption intensity (Heiken 1972; Gonnermann and Manga, 2006; Cashman and Rust 2016;
152 Walowski et al., 2019).

153 In terms of particle morphology, complex condensation processes in volcanic plumes
154 can lead to the formation of particles with widely varying forms from perfect spheres to
155 more 'fluffy' ash aggregates (e.g. Obenholzner et al. 2003). Particles may precipitate as a
156 single homogeneous phase at high temperatures, but may also have multiphase histories
157 forming aggregates from interactions during eruption and deposition (Mather et al. 2003;
158 Obenholzner et al. 2003). The morphology of the products of the liquid phases on
159 condensation vary from droplets (tailed spherules) to perfect spheres (Elkins-Tanton et al.
160 2003).

161 Particles can also grow by agglutination and interact with other particles in the
162 volcanic plume (Heiken 1972). Spherules can be solid (plerospheres) or hollow
163 (cenospheres) with sizes varying from <1 µm to 1000s µm (Moune et al. 2007; Porritt et al.
164 2012). In different volcanic centres fallout ash and condensates can contain volcanic
165 particles of both magmatic and non-magmatic origin; for example at Popocatépetl (Mexico;
166 Obenholzner et al. 2003); Masaya (Nicaragua; Martin et al. 2009) and Mount Etna (Italy;
167 Martin et al. 2008). Ash particles have variable size distributions, with hydromagmatic,
168 explosive ash forming smaller particles due to efficient fragmentation (e.g. Eyjafjallajökull;
169 Gislason et al. 2011) than those formed during other types of eruptions; e.g. Plinian type at
170 Masaya (Martin et al., 2009). Finally lithic fragments can be rounded by particles interacting
171 and abrading during the eruption.

172 Achneliths (small black glass particles) are described in many basaltic eruption
173 products where ash- to lapilli-size pyroclasts are formed during Strombolian to Hawaiian
174 type events (Moune et al. 2007; Porritt et al. 2012). Achneliths can be found associated with
175 subaerial, small, monogenetic volcanoes, in Strombolian scoria cones and in tephra
176 generated in hydrovolcanic explosions (Porritt et al. 2012; Carracedo-Sánchez et al. 2016).
177 The shape of an achnelith is controlled by the acceleration of melt blebs during eruption,
178 surface tension and air friction (Moune et al. 2007). Spherical to near-spherical or pear-
179 shaped droplets of magma with glassy exteriors are termed Pele's tears (Heiken 1972;
180 Porritt et al. 2012). Surfaces of Pele's tears can show contraction joints, be smooth or show
181 evidence of interaction with other particles during transport in the volcanic plume (Heiken

1972; Moune et al. 2007). Pele's spheres from Kilauea Iki (Hawaii) tend to be <1-2 mm in size and are vesiculated with limited crystal content (Porritt et al. 2012). At Masaya (Nicaragua) the spherical pyroclasts are smaller (<600 μm) and the outer surfaces are rough with small particles adhering to them (Moune et al. 2007). Vesiculation is a key feature of pyroclast morphology depending on droplet size. Larger droplets vesiculate to form bread crust tears and scoria, while smaller droplets form spheres and tears (Porritt et al. 2012). The presence of spherical particles is characteristic of low viscosity magmas (Heiken 1972; Porritt et al. 2012).

In tephra deposits, individual spheres or clusters of spheres can have distinct chemical compositions depending on their source and the degree of interaction that takes place during eruption. For example, the chemical composition of spherical particles from the plume of Popocatépetl volcano included variable amounts of major elements (Si, Al, Ca, Fe etc), some transition metals (Cu, Zn, Ni, V) and non-metals (S, O, Cl) (Obenholzner et al. 2003). Volcanic spherules are commonly composed of glass with chemical compositions varying from that of the erupted magma to nearly pure SiO_2 (Moune et al. 2007; Porritt et al. 2012; Glass 2016). Most achneliths are basaltic or basaltic andesite in composition; however Pele's tears exhibit wide chemical variability varying from 47–98 wt.% SiO_2 (Moune et al. 2007). Chemical zonation and enrichment in silica towards the rims of some tears has been attributed to the interaction of silicate droplets with acid gases inside the volcanic plume (Carracedo-Sánchez et al. 2016).

In recent years several studies have focused on the fine particles collected in volcanic plumes (e.g. Etna, Masaya; Martin et al. 2008, 2009) and generated by volcanic lightning (Genereau et al. 2015; Wadsworth et al. 2017). Here we describe rare spherules and spheroidal particles from three different tephra deposits in Argentina and report the range of chemical composition found at each location in order to determine their mode of formation.

Geological setting of the Payenia volcanic province

The Payenia volcanic province is part of the Andean southern volcanic zone and stretches between 34 and 38°S (Litvak et al. 2018). Volcanism in the region is related to subduction of the Nazca plate beneath the South American continent and occurs up to 550 km east of the

trench (Jones et al. 2016). A major Late Pliocene change in subduction geometry from shallow (<30°) to normal (~30°) slab dips beneath the province resulted in volcanism characterised by alkali basalts displaying typical back-arc compositions with variable slab input (Søager et al. 2015; Litvak et al. 2018). Within the Payenia province, over 800 mono- and polygenetic centres extend over an area of ~40,000 km^2 (Folguera et al. 2009; Pallares et al. 2016). The southern limit is defined by the Cortaderas lineament (Figure 1), which developed in the Miocene (Ramos and Kay, 2006). Both pre-existing basement faults and fractures as well as extension-related structures are thought to have influenced the distribution of the volcanic centres (Ramos and Kay, 2006), and to have favoured rapid eruption over a wide area (Kay et al. 2005). The Payenia volcanic province can be divided into northern, central and southern regions, each with distinct mantle sources (Brandt et al. 2017). Unusual tephra samples from two of the southern volcanic centres (Auca Mahuida and Tromen; Pallares et al. 2019) between latitudes of 37°S and 38°S, south of the Rio Colorado in Argentina are the focus of this study (Figure 1). The two volcanic fields appear to be aligned parallel to the Cortaderas lineament and are considered to be influenced by enriched mantle and variable degrees of melting (Wieser et al. 2019). The volcanic centres erupted through Mesozoic to Palaeogene sediments of the Neuquén basin (Søager et al. 2015). The basin contains up to 4000 m of a mixed siliclastic-carbonate succession, which has been deformed over time as the region switched between extensional and compressional stress regimes (Jones et al. 2016).

Auca Mahuida and Tromen volcanic systems

The Auca Mahuida shield volcano is part of the southernmost major volcanic centre in the Payenia province and is located close to the north-west-trending Cortaderas lineament (Figure 1). The Auca Mahuida volcano was constructed in the Pleistocene from 1.8 to 1.0 Ma during five volcanic phases, covers an area of ~45 km^2 and includes pyroclastic cones and a shield volcano (Pallares et al. 2016). The Auca Mahuida central cone is 11 x 15 km and the summit caldera is ~2 km wide at an elevation of 2250 m (Pallares et al. 2016). Chemical composition of erupted lavas varies from alkali basalt to trachyte (Hernando et al. 2014; Pallares et al. 2016).

The Tromen volcano is located to the NW of Auca Mahuida (Figure 1). The Tromen volcanic system dates from the Pliocene (4.04±0.4 Ma), with the last phase of activity at

175±35 ka (Kay et al. 2006; Folguera et al. 2009). It is a composite volcano built of several volcanic edifices. The youngest volcanic vents include a series of Late Quaternary polygenetic and monogenetic volcanoes and domes composed of basalt and andesite. The vents are conical in form and at an elevation of ~2500 m. Magmatism at Tromen is predominantly transitional in composition (Pallares et al. 2019). There is evidence of multiple episodes of partial melting and interaction of the magma with crustal material and mixing (Kay et al. 2013).

Samples

Tephra samples were collected from several different volcanic centres in the Payenia volcanic province with an original aim of understanding the geochemistry of the Payenia region (e.g. Wieser et al. 2019). Approximately 1 kg of material was collected from each of the sampled monogenetic scoria cones or from individual scoria layers in quarried sections. Particle sizes varied from <10 μm to >6 mm. Here we focus on the spherules and spherical particles that were found during processing in three of the 35 original samples collected (NQN2 (Tromen), NQN4 and NQN5 (Auca Mahuida)) in southern Payenia (Figure 1). The spherules are not widely distributed but warranted further investigation due to their morphology and distribution.

Methods

The tephra samples were initially examined using a stereomicroscope, and spherical/spheroidal particles were separated. A cone-splitting technique was used to separate a subset of the tephra sample for X-ray fluorescence (XRF) analysis. Glass discs and powder pellets were then prepared for major element oxide and trace element analyses, respectively, of the tephra. Standards BCR-1, JA-2, BHVO-1 and BIR-1 were analysed at the same time. Based on the repeated analysis of standard BHVO-1 and an individual tephra sample, the precision for the major element analysis is determined as <1.1% (1σ). Accuracy as indicated by % difference to published values of BHVO-1 (Govindaraju, 1994) is within 1%.

The separated spherical/spheroidal particles were mounted in epoxy resin, polished, and initially coated with carbon. Their major element chemical composition was then

determined using the Cameca SX-100 electron microprobe at the University of Edinburgh. Analyses were performed using a 5 μm beam and an accelerating voltage of 15 kV. A low beam current of 1 nA was used as an added precaution against Na mobilisation. The following standards were utilized for calibration: jadeite for Na, spinel for Mg and Al, orthoclase for K, wollastonite for Si and Ca, synthetic fayalite for Fe, Durango apatite for P, rutile for Ti, and pure metals for Mn, Cr and Ni. Cameca software, PeakSight, was used to process data after collection, and analyses with poor totals (outside of the range 97-101%), were not included in the final dataset. See supplementary file A for full dataset and individual analyses totals. Elements were analysed in the following order: Na, Mg, Al, Si, K, K, Ca, Fe, Ca, P, Ti, Mn, P, Ti. See supplementary file A for full dataset. Three sigma standard deviation was <0.1 wt.% for Mg, K, Mn, Cl, P, S, Ti, F; <0.3 wt.% for Al, Ca, Fe; <0.5 wt.% for Na and <1 wt.% for Si.

High resolution backscatter and secondary electron images of the polished spherical particles were acquired using a Zeiss SIGMA HDVP FEG scanning electron microscope at the School of GeoSciences, University of Edinburgh using a 20 kV accelerating voltage, a 70 μm aperture size and a 7 mm working distance. The Oxford AZtecEnergy dispersive X-ray analysis system was used to generate major element maps of some of the perfect spheres. Selected carbonate spheroids were analysed using the Cameca imf 4f facility at the University of Edinburgh. The SEM mounts were cleaned and coated in Au. Secondary positive ions were produced by sputtering the sample surface with a 5 nA primary beam of $^{16}O^-$. The secondary ions were accelerated by 4.5 kV and counted by a single EM detector. An energy window of 42 eV was used. The analyses were carried out at a 75 V offset so that only the high-energy ions were detected and molecular interferences were reduced. An internal laboratory standard OKA-Buse was used and the selected elements (Mg, Ca, Sr, Y, Nb, Ba, La, Ce, Nd) analysed. See supplementary file A for full dataset. Following analysis the gold coating was removed and further images acquired.

Results – Tephra composition and spherical particle morphology

The samples in which the spherules were found are all highly vesiculated and can be described as tephra consisting predominantly of lapilli (~70%), volcanic ash (~20%) (Figure

2), volcanic breccia and agglomerate (~10%). The samples are fresh in appearance with minor oxidation and little evidence of alteration. Mineralogy determined optically includes olivine, pyroxene and plagioclase phenocrysts, iron oxides and apatite as well as glass and lithic fragments. This is similar to the olivine, clinopyroxene, and oxide phenocrysts and microcrysts of plagioclase and alkali feldspar found in scoria from other parts of the Payenia province (Wieser et al. 2019). The Tromen sample contains plagioclase (15%), olivine (~5%) and clinopyroxene (~5%). The plagioclase and olivine are <2 mm in size, clinopyroxene is smaller <450 μm and commonly zoned. Plagioclase composition ranges from andesine to labradorite. The Auca Mahuida samples have a similar modal mineralogy but slightly larger clinopyroxene phenocrysts (up to 1 mm). Plagioclase is more Na-rich and varies from oligoclase to andesine in composition. The spherical/spheroidal particles are randomly distributed in the volcanic ash (Figure 2), only the white spheroidal particles are recognised in thin section (Figure 2).

All the analysed tephra are mafic in composition with SiO_2 ranging from 45 to 49 wt.% (Table 1). The Tromen tephra sample is compositionally distinct from those from the Auca Mahuida volcanic field with higher SiO_2, Al_2O_3, CaO, Na_2O, and lower TiO_2, MgO, K_2O and P_2O_5 (Table 1).

Four different types of spherical particles were observed using a stereomicroscope in three tephra samples, but none was found in any of the other volcanic ash samples collected throughout the region. The spheroidal particles range in size from ~50 μm to 220 μm in diameter and are transparent, milky white, dark green or black in colour. Only the transparent spherules are perfect spheres (Figure 3). Other morphologies include spheroids, ellipsoids and dumbbells. The smooth, rounded surfaces of some of the spherules suggests surface tension was important during formation (Figure 3) and can help establish their origin (Mutch 1964).

There is a distinct morphological variation in the spherical particles depending on which sample is examined. NQN2 from Tromen contains perfectly rounded and transparent spheres that occasionally form aggregates, possibly through budding (Figure 3). These smooth spheres have the smallest surface area for a given volume and no obvious surface features. Milky white, more ellipsoidal particles as well as black and green spheroidal particles are also observed. NQN4 (Auca Mahuida) contains a similar mixture of particle

morphologies whilst NQN5 is dominated by carbonate particles (Figure 3). The transparent spherules are either hollow or contain a single holocrystalline phase (Figure 4). Only the milky white spherules were evident in thin sections where they are seen to be carbonate in composition, are concentrated in small areas and are not ubiquitous (Figure 5). The vesicles in the tephra are empty (Figure 2), and a few of the spheroidal particles showed limited evidence of vesiculation.

Chemical composition of the spherical particles

A number of spherules/spheroids separated from the tephra samples were analysed at both the core and the rim in order to ascertain the chemical diversity of individual particles (Table 2, Figure 4). Compositionally the spherules and spheroidal particles are extremely variable with four distinct groups: (i) silica-rich spherules; (ii) mafic spherules/spheroids; (iii) Fe-rich spheroids; and (iv) carbonate spheroids. Average compositional data for the Si-rich and mafic spherules are presented in Table 2, and the full dataset is given in supplementary file A.

(i) *Silica-rich spherules*: These are transparent and range in composition from 72 to 75 wt.% SiO_2. They have exceptionally low Al_2O_3 for silicate glasses (0.2 to 2.0 wt.%) and high Na_2O (12 to 16 wt.%) and CaO (6.6 to 12.2 wt.%) contents (Table 2; Supplementary file A). There is little variation in composition between the core and the rim of each of the spherules (Table 2, Figure 6, 7a). However greater variation is seen between the composition of individual spherules from the same sample; e.g. CaO, MgO, Na_2O, F contents (Table 2). Each spherule is distinctive in composition, but remarkable consistency is seen in the repeat spot analyses obtained for each spherule (Figure 7a).

(ii) *Mafic spherules/droplets*: The dark green/brown droplets are mafic in composition with SiO_2 ranging from 39.5 to 48.9 wt.%. One of the two different spheroids measured from sample NQN4, Spherule B, is fairly homogeneous from core to rim and is similar in composition to the rim of Spherule C, while the core of Spherule C is distinctly different, composed primarily of SiO_2 (39.5wt.%), MgO (40.2 wt.%) and FeO (18.8 wt.%) (Table 2). These spheroids contain abundant crystallites of olivine primarily and vesicles which we attempted to avoid during analysis. The core of Spherule C is similar in composition to olivine (Table 2,

Figure 7a). The composition of the Andean spheroids is distinctly different to the overall composition of the tephra in which they are found (Table 1, NQN4). The spherules are more than 1 wt.% higher in SiO_2, TiO_2, Al_2O_3, Na_2O, K_2O and ~5 wt.% lower in MgO (Table 1, 2) than the host tephra.

(iii) *Fe-rich spheroids*: These black spheroids mainly contain FeO (~75wt.%), TiO_2 (~12.5wt.%), MgO (3.6 wt.%) and Al_2O_3 (3.5 wt.%) (Table 2). They are similar in composition to titanomagnetite. The Fe-rich spheroids lack evidence of vesiculation or other recognisable surface characteristics.

(iv) *Carbonate spheroids*: The majority of the spheroids from sample NQN4 and NQN5 are carbonate in composition. The carbonate is heterogenous in composition (Figure 4), with notable variation in S content in particular (Table 2). The question arises as to whether these spheroids are primary or secondary in nature. All the spheroids appear to form either from a single calcite crystal or are crystal aggregates. In thin section the carbonate spheroids appear to be concentrated in particular regions and to co-exist with empty vesicles (Figure 2). The samples are completely unaltered and the carbonate spheroids occasionally have dumbbell forms (Figures 4, 5). Trace element analyses of the carbonate spheroids from NQN5 indicate two populations. The first has elevated Sr/Y (673-1257) and Ba/La (0.73-11), while the second has low Sr/Y (136-385) and Ba/La (0.58-1.72), consistent with the higher overall concentrations of trace elements in the second population (Table 3).

Discussion

There is a variable amount of data in the literature concerning the form and composition of spherules and spheroidal particles formed by different processes; e.g. impact related, volcanic lightning or magmatic.

Morphology of spherules and their different origins in a volcanic plume

The Weber number ($W_e=\rho_l d_0 u_0^2/\sigma$, where ρ_l = density of liquid, d = droplet diameter, u_0 = droplet fall velocity and σ = surface tension of liquid) describes droplet fall and resultant form (Misyura 2017). Experimental studies of the formation and breakup of liquid droplets indicate that a low W_e together with a large Reynolds number results in the formation of

droplets (Porritt et al. 2012). This is consistent with observations of particle morphology being dependent on surface tension, air friction and particle velocity on eruption (Heiken 1972). The transformation from a droplet to dumbbell during a tumbling motion occurs at a constant speed of rotation (Elkins-Tanton et al., 2003). Molten melt experiments have shown that non-equilibrium teardrop forms can arise from the breakup of dumbbell shapes (Elkins-Tanton et al., 2003). This is evident from tektites that typically assume the forms of bodies of revolution, specifically spheres, ellipsoids, dumbbells, and even tori. The morphology of the spherules and spheroids examined during this study indicate that processes related to the eruption dynamics were important in dictating the forms observed and that many are primary. The range in spherule types, notably dumbbells, paired/joined and tear-shaped testifies to formation of droplets in a high-density plume environment.

Based on observations from Suswa volcano (Kenya) Macdonald et al. (1993) proposed several textural and mineralogical lines of evidence to determine if carbonate spheroids were primary (i.e. magmatic in origin), rather than associated with later alteration processes. The criteria include: the presence of coalescing carbonate spheres; some flattening of carbonate spheres; lack of carbonate veining or alteration of rock fragments; lack of compositional zonation of the calcites which would be expected if formed from migrating fluids; and the presence of carbonate globules in fresh silicate glass inclusions within phenocrysts.

The carbonate spherules in the Payenia samples satisfy many of the above criteria (Figures 4, 5); including coalescing spheres, flattening of some spheres, and no veining or well-developed zonation, suggesting formation related to magmatic processes. Their random distribution in the tephra is consistent with being co-magmatic rather than late-stage alteration products. Furthermore, sample NQN4 also contains completely hollow carbonate spheres, this is consistent with formation from supercritical fluids rather than as a late-stage infill. The calcite does not transgress the margins of the spheroids nor is there evidence of radial growth (Figure 4), both of which would, if present, suggest a secondary rather than magmatic origin (Wallace et al. 1990). We suggest that the carbonate is of primary origin based on these observations and explore the potential for an origin from supercritical hydrous fluids. We now compare our new geochemical data with those reported in a number of different studies documenting both similarities and differences.

Comparison with non-volcanic spherules

There are a number of distinctive micrometeorite, microtektite, impact and ablation spherule compositions varying from Fe-rich (>70 wt.% FeO) and Fe-sulphide particles (e.g. Schulte et al. 2003; Genge et al., 2008; Wu et al. 2013; Orgeira et al. 2017; Ohtaki et al. 2019), to carbonate-rich (e.g. Graup, 1999; Schulte et al. 2003) and K-rich (Schulte et al. 2003). Tektites and microtektites tend to be Si-rich (63-81 wt. % SiO_2) and Na-poor (Folco et al. 2016; Glass 2016).

All reported non-volcanic spherule compositions are distinctively different to those measured from the Payenia volcanic province. For example, Fe-rich micrometeorites have similar Fe contents but contain no Ti, or they have lower Fe and Si (Schulte et al. 2003; Genge et al. 2017; Ohtaki et al. 2019). None of the samples from Payenia has a chondritic composition similar to silicate-dominated S-type spherules, and K-rich spherules were not observed from Payenia. Furthermore there is no evidence of surface textures such as well-developed crystalline dendrites or regular polygonal textures of equant crystals which are characteristic of cosmic spherules (Mutch 1964).

Where carbonate spherules from impact sites (e.g. Acraman, Australia) are reported some are clearly diagenetic (e.g. Wallace et al. 1990), while others are indicative of carbonate-silicate melt immiscibility (e.g. Schulte et al. 2003). Where carbonate-silicate immiscibility has been recorded, carbonaceous sediments in the impact layer have melted and were the source of CaO and CO_2 (Graup 1999; Schulte et al. 2003). Evidence to support a primary impact origin of the spherules includes coalesced carbonate globules, lack of traces of later infilling of vesicles and sharp boundaries between spherules (Schulte et al. 2003). The resultant carbonate spherules have low trace element concentrations due to the sedimentary origin of the Ca. The concentration of some trace elements, notably Sr and Ba, in the carbonate spheroids from Payenia is higher than found in sedimentary carbonates (Table 3), and are remarkably different to those derived from alkaline magmas, which suggests the Payenia spheroids have not been formed by liquid immiscibilty.

The major element composition of normal microtektites contain high contents of silica (SiO_2 ~60 -78 wt%) and alumina (Al_2O_3 > 12 wt.%), low total alkali element contents (0.50–1.85 wt.%), and MgO abundances <5 wt.% (Folco et al. 2009). High-Mg microtektites from Antarctica contain SiO_2 ~60 wt.%, >15.wt.% Al_2O_3 and MgO >10 wt.% (Folco et al. 2009). In Payenia the composition of the Si-rich spherules is distinctively different from that

reported for tektites and rhyoltic glasses (Folco et al. 2009; Glass 2016) as the Payenia high-Si spherules have very low (<2.0 wt.%) Al_2O_3.

The Payenia silica-rich spherules have a very distinctive composition that is surprisingly similar to that of manufactured soda-lime glass in terms of SiO_2, Al_2O_3 and Na_2O (Mueller et al. 2017) but with higher TiO_2, CaO, FeO, and K_2O, and quite unlike previously reported natural silica-rich glasses (e.g. Glass, 2006).

Comparison with magmatic spherules

The composition of volcanic spherules reported from Hawaii, Kenya, Nicaragua and Spain is relatively diverse (Figure 7b). The spherules from Hawaii are Si-rich (55-95 wt.% SiO_2) relative to host tephra composition (Figure 7b) and span a wide range in major element composition e.g. MgO: 7.2 - 0.1 wt.%; Al_2O_3: 20 - 0.4 wt.%; CaO: 10 - 0.5 wt.% (Meeker and Hinkley 1993). These spheres are dominated by SiO_2, whilst some spherules appear zoned (Meeker and Hinkley 1993). Glass spherules from Calatrava, Spain are mafic to intermediate in composition (45 – 59 wt.% SiO_2) and also show large-scale variability in major-element compositions e.g. CaO: 1.9 – 17.9 wt.% (Carracedo Sánchez et al. 2015) (Figure 7b). Spherules (Pele's tears) from Masaya (Nicaragua) are zoned in composition varying from Si-rich rims to intermediate composition cores (Moune et al. 2007). The core composition of these Masaya Pele's tears are considered to be unaffected by dissolution of the silicate glass during interaction with volcanic gases in the plume (Moune et al. 2007). Surface alteration leads to an increase in Si, Al, Fe and Ti and a decrease in K, Na, Ca, Mg due to the different mobility of network-forming and network-modifying cations (Sterpenich and Libourel 2001; Moune et al. 2007). The unaltered composition measured at Masaya is similar in composition to the mafic droplets from Payenia (Figure 7b). Finally globules reported from ash-flow tuffs in Kenya are both silicate and carbonate in composition (Macdonald et al. 1993) and show some superficial similarity to the high-Si and carbonate spherules recorded in the Payenia region of the Andes (Figure 7b).

The Suswa volcano in the central Kenya Rift valley is highly alkaline in composition and shows evidence of silicate-carbonate melt immiscibility (Macdonald et al. 1993). The volcano is Pleistocene in age with good evidence of explosive activity (ashes, pumice lapilli airfalls and carbonate-trachyte ash flows) (Macdonald et al. 1993). Silicate spherules from Suswa are more evolved (59-64 wt.% SiO_2) than the host lava (56-57 wt.% SiO_2). A

relationship between spherule size and composition has been proposed as larger spherules tend to be mildly peralkaline, while the smaller ones are metaluminous. Macdonald et al. (1993) argue this is because smaller spherules form by marginal budding from larger spherules resulting in a trend of decreasing peralkalinity due to Na loss and increasing silica-oversaturation with decreasing size. The Payenia spherules show some similarities. For example, the spherules are more evolved by comparison to the host lava and all silicate spherules are silica-oversaturated, however the Payenia spherules are either more Si-rich (NQN2) or are similar in Si content to the host lava (NQN4) (Tables 1, 2) (Figure 7b) and have remarkably low Al contents.

In Suswa (Kenya), the carbonate spherules (46-52 wt.% CaO) all contain low abundances of SiO_2, Na_2O and FeO_T and high F (0.55 to 1.38 wt. %) which was used to strongly suggest a magmatic origin for the carbonate (Macdonald et al. 1993). The Payenia carbonate spheroids are almost pure $CaCO_3$ with only trace amounts of other elements including Si, Mg, Al, Fe, P and S (Table 2). The Payenia carbonate spherules also have modest amounts of some trace elements (e.g. Sr), but much lower than calcite in Ca-carbonatite (Table 3) indicating that they have been generated by different processes.

The solubility of volatiles including water and CO_2 in magmatic systems depends on temperature, pressure, melt composition and oxygen fugacity (Gonnermann and Manga 2006; Walowski et al. 2019). Most melts are thought to be saturated in volatiles at the point of eruption (Gonnermann and Manga 2006). At temperatures >31 °C and pressures >7 MPa CO_2 is a supercritical fluid; the corresponding values for water are 374°C and 22 MPa. Consequently mixtures of water and CO_2 will be supercritical at depths greater than about 0.5 km at magmatic temperatures, the exact depth depending on the molecular ratio of H_2O:CO_2. These supercritical fluids will have low density and enhanced solvent capacity for silicates. When a magma containing dissolved water and CO_2 rises toward the surface it will eventually become volatile-oversaturated and exsolve a silicate- and carbonate-saturated supercritical fluid. As the magma erupts the fluid will flash into vapour and precipitate its dissolved components as tiny spherical droplets of immiscible silicate and carbonate (Figure 8).

The most persuasive evidence for the involvement of supercritical hydrous fluids is provided by the composition of the silica-rich glass spheres. As was noted earlier, these are

chemically similar to soda-lime glass, with high Si, Ca and Na, but very low Al (Al_2O_3 = 1.1–1.8 wt.%). Their highly peralkaline composition (atomic (Na+K)/Al = 15–19) is well outside the range of peralkaline igneous rocks where atomic (Na+K)/Al rarely exceeds 2 (Macdonald 1974; Marks and Markl 2017). The very low concentration of Al_2O_3, coupled with high concentrations of SiO_2, CaO and Na_2O, reflects the relative solubility of these oxides in supercritical water (Walther 1968). We therefore interpret the silica-rich glass spheres as condensates from supercritical magmatic fluid as it depressurised on eruption. A similar origin is proposed for the carbonate spheroids.

The Fe-rich spheroids resemble titanomagnetite in composition and may have been rounded during the eruptive process. Titanomagnetite can be formed towards the end of the crystallization sequence, mostly driven by volatile exsolution (Mollo et al. 2015). Compositionally these spherules are very different to the Fe-rich spherules reported from lunar soils and the Chicxulub ejecta sites as they contain significantly high Ti and lack S (Schulte et al. 2003; Orgeira et al. 2017; Ohtaki et al. 2019). No surface features have been recognised on these spheroids. Furthermore, the composition is very different to the host tephra.

Finally, the mafic spheroids contain some vesiculation and microlites consistent with a mode of formation similar to Pele's tears as found for example at Hawaii and Nicaragua.

A mechanism for generating heterogeneous spherules in the Payenia volcanic province

All magmatic systems contain volatiles, which partition into a fluid phase at low pressures (Figure 8). Once a magma is fluid-saturated, unmixing can occur which can influence factors such as composition and eruption dynamics (Cashman and Rust 2016). Immiscible CO_2 fluids are most common in basaltic systems and the liberation of CO_2 following crustal carbonate assimilation can result in explosive eruption behaviour as during the Merapi (Indonesia) 2010 eruption (Deegan et al. 2010). Other volcanic systems emplaced in carbonate-rich crust that display explosive volcanic behaviour include the Alban Hills (Italy), Vesuvius (Italy) and Popocatépetl (Mexico) (Freda et al. 1997; Del Moro et al. 2001; Schaaf et al. 2005). Excess CO_2 is common in these systems and may originate from the thermal decomposition of wall-rock carbonates, crustal decarbonation and assimilation (Deegan et al. 2010; Spandler et al. 2012). Evidence of diffusive loss of H^+ includes high CO_2/H_2O ratios in melt inclusions and the precipitation of magnetite (Preece et al. 2014). We find titanomagnetite

554 spheroids associated with carbonate spheroids in sample NQN4. Unfortunately we do not
555 know whether melt inclusions in the tephra are particularly CO_2-rich, but amphibole has
556 been described from volcanic rocks in Auca Mahuida (Kay et al. 2013) and apatite was found
557 as an accessory phase in these tephras which suggests a volatile-rich initial melt.
558 Prior to the Payenia eruptions at Auca Mahuida, CO_2 degassing and the interaction of
559 melt and volatiles with the surrounding carbonate host rock may have led to the formation
560 of an unusually CO_2-rich supercritical hydrous fluid phase (Figure 8). This fluid would contain
561 high concentrations of those elements that are soluble in supercritical water (notably Si, Ca
562 and Na, but not Al). As the magma rose to shallow levels, the release of fluid as vapour
563 would drive a violent eruption leading to the tephra deposits observed. The supercritical
564 fluid phase would lose its solvent ability as it flashed into steam and its cargo of dissolved Si,
565 Ca and Na would condense as immiscible silica-rich and carbonate droplets.
566 We suggest that the presence of late-stage supercritical CO_2-rich hydrous fluids can
567 lead to the formation of carbonate and unusual silica-rich spherules during explosive
568 eruptions. The association of separate Fe-rich and mafic spherules is potentially more
569 common and is consistent with volatile degassing and violent eruption dynamics as
570 recognised in other explosive eruption centres such as Etna and Masaya (Martin et al. 2008;
571 Martin et al. 2009). Melt products from lightning arc experiments (Mueller et al. 2018)
572 indicate loss of Na, P, S and F but otherwise little variation from the starting glass
573 compositions, with no reported Al loss. This suggests that it is more likely that the explosive
574 eruption dynamics in the presence of CO_2-rich supercritical hydrous fluids resulted in the
575 formation of the array of particle forms observed.
576
577 *Conclusions*
578 The four different types of spherule and spheroidal particles found in tephra from the
579 Payenia volcanic province of the Andes are all volcanic in origin and form as a result of
580 segregation of supercritical fluids followed by syn-eruptive condensation processes. Their
581 compositions are distinctly different from spherules formed by the impact or atmospheric
582 melting of extra-terrestrial material. The spherule compositions are diverse ranging from
583 high-Si glasses to silicate melts similar in composition to the host tephra, and from
584 carbonate to Fe-Ti rich globules. Carbonate is the principal CO_2 carrying mineral phase in the
585 crust. Magmatic CO_2, and carbonate-hydrous fluids formed possibly through interaction

586 with carbonate in the basement are key to the formation of the carbonate and Si-rich
587 spherules. We conclude that mechanisms including rapid condensation on eruption led to
588 the formation of the spherules from supercritical fluids. Crustal carbonate dissolution may
589 be an additional important source of CO_2 outgassing and should not be ignored in
590 calculating CO_2 mass balances.

591 Figure captions

592 Figure 1. Annotated Google Earth image showing location of tephra samples adjacent to the
593 Tromen and Aucun Mahuida volcanic centres in Argentina, South America. Major structures
594 include the Cortaderas lineament (after Pallares et al. 2019).

595 Figure 2. (a) and (b) Spheroidal particles and mineral phases within the tephra sample NQN2
596 from the Tromen volcanic field. Image is from loose material examined under
597 stereomicroscope. Note the variability in form of the spherules from perfect spheres to
598 aggregates. (c) and (d) Thin section photomicrograph (in plane-polarised light and with
599 crossed polars) of volcanic ash fragment from NQN5. Note the presence of carbonate
600 spheroidal particles adjacent to vesicles. Olivine and plagioclase are the major phenocryst
601 phases, set in a glassy matrix.

602 Figure 3. Morphology of different spherical particles separated from the different tephra
603 samples. Forms include perfect spheres, aggregates, droplets varying from transparent to
604 brown glasses. Size of particles >200 microns.

605 Figure 4. Backscatter and secondary electron images of indiviual spherules. (a) Unfilled
606 carbonate spherule (NQN4); (b) Dumbbell-shaped calcite showing heterogeneous chemical
607 composition (NQN4); (c) Perfect Si-rich spherule (NQN2 Spherule F); Note small round
608 circles are the damage caused by electron microprobe analyses highlighted by remnant gold
609 coating.

610 Figure 5. Carbonate spherules in thin section NQN5. Note the dumbbell form in addition to
611 the spheroidal calcite.

612 Figure 6. Major element maps of Si-rich spherule NQN2 (F) highlighting the compositional
613 homogeneity. Note black circles are marks from EMPA showing position of original analyses.

614 Figure 7a. CaO (wt.%) versus SiO_2 (wt.%) comparison of multiple spot analyses of selected
615 silicate spherules from the Payenia region. Core (filled dark symbol) and rim (open white or
616 grey symbol) compositions show little variation within individual spherules with the
617 exception of spherule NQN4-C. Carbonate and Fe-rich spherules (with < 0.2 wt.% SiO_2) are
618 not included.

Figure 7b. Comparison of average data from spherules in the Payenia region with volcanic spherules from Kenya, Spain, Nicaragua and Hawaii. Selected data from Carracedo Sánchez et al. 2015; Macdonald et al. 1993; Meeker and Hinkley 1993; Moune et al. 2007; Porritt et al. 2012. Note the comparison between the Kenya samples (Macdonald et al. 1993) and those from Payenia (this study).

Figure 8. Schematic figure showing the relationship between volatile degassing, supercritical hydrous fluids, eruption dynamics and spherule formation. Immiscible silicate and carbonate spherules condense from CO_2-rich supercritical hydrous fluids resulting in distinctive spherule compositions including the low Al contents of Si-rich spherules. The mafic and Fe-rich spherules are formed in the plume.

Acknowledgements: The authors acknowledge NERC grant 'Mantle volatiles: processes, reservoirs and fluxes' (NE/M000443/1) for funding. Mike Hall, Nicola Cayzer and Chris Hayward are thanked for their help with mount preparation, SEM and EPMA respectively. Nic Odling is appreciated for support with XRF analyses is appreciated and John Craven for IMF support. We are particularly grateful for the expert reviews by M.D. Suttle and K. Genareau which greatly improved the manuscript.

Supplementary material. Appendix A contains the full analytical dataset collected by EPMA and SIMS.

References:

Brooker, R.A. & Kjarsgaard, B.A. 2010. Silicate–Carbonate Liquid Immiscibility and Phase Relations in the System SiO2–Na2O–Al2O3–CaO–CO2 at 0·1–2·5 GPa with Applications to Carbonatite Genesis. *Journal of Petrology*, **52**, 1281-1305, doi: 10.1093/petrology/egq081.

Carracedo-Sánchez, M., Sarrionandia, F., Arostegui, J., Errandonea-Martin, J. & Gil-Ibarguchi, J.I. 2016. Petrography and geochemistry of achnelithic tephra from Las Herrerías Volcano (Calatrava volcanic field, Spain): Formation of nephelinitic achneliths and post-depositional glass alteration. *Journal of Volcanology and Geothermal Research*, **327**, 484-502, doi:10.1016/j.jvolgeores.2016.09.006.

Carracedo Sánchez, M., Sarrionandia, F., Arostegui, J. & Gil Ibarguchi, J.I. 2015. Silicate glass micro and nanospherules generated in explosive eruptions of ultrabasic magmas: Implications for the origin of pelletal lapilli. *Journal of Volcanology and Geothermal Research*, **293**, 13-24, doi: 10.1016/j.jvolgeores.2014.12.010.

Cashman, K. & Rust, A. 2016. Introduction. *In*: Mackie, S., Cashman, K., Ricketts, H., Rust, A. & Watson, M. (eds.) *Volcanic Ash*. Elsevier, 5-22.

Deegan, F.M., Troll, V.R., Freda, C., Misiti, V., Chadwick, J.P., McLeod, C.L. & Davidson, J.P. 2010. Magma–Carbonate Interaction Processes and Associated CO2 Release at Merapi Volcano, Indonesia: Insights from Experimental Petrology. *Journal of Petrology*, **51**, 1027-1051, doi: 10.1093/petrology/egq010.

Del Moro, A., Fulignati, P., Marianelli, P. & Sbrana, A. 2001. Magma contamination by direct wall rock interaction: constraints from xenoliths from the walls of a carbonate-hosted magma chamber (Vesuvius 1944 eruption). *Journal of Volcanology and Geothermal Research*, **112**, 15-24, doi: https://doi.org/10.1016/S0377-0273(01)00231-1.

Elkins-Tanton, L.T., Aussillous, P., Bico, J., QuÉRÉ, D. & Bush, J.W.M. 2003. A laboratory model of splash-form tektites. *Meteoritics & Planetary Science*, **38**, 1331-1340, doi: 10.1111/j.1945-5100.2003.tb00317.x.

Essene E.J., Fisher D.C. 1986. Lightning strike fusion: extreme reduction and metal-silicate liquid immiscibility. *Science*, **234**,189–193.

Folco, L., D'Orazio, M., Gemelli, M. & Rochette, P. 2016. Stretching out the Australasian microtektite strewn field in Victoria Land Transantarctic Mountains. *Polar Science*, **10**, 147-159, doi: https://doi.org/10.1016/j.polar.2016.02.004.

Folco, L., D'Orazio, M., Tiepolo, M., Tonarini, S., Ottolini, L., Perchiazzi, N., Rochette, P. & Glass, B.P. 2009. Transantarctic Mountain microtektites: Geochemical affinity with Australasian microtektites. *Geochimica et Cosmochimica Acta*, **73**, 3694-3722, doi: https://doi.org/10.1016/j.gca.2009.03.021.

Folguera, A., Naranjo, J.A., Orihashi, Y., Sumino, H., Nagao, K., Polanco, E. & Ramos, V.A. 2009. Retroarc volcanism in the northern San Rafael Block (34–35 30' S), southern Central Andes: Occurrence, age, and tectonic setting. *Journal of Volcanology & Geothermal Research*, **186**, 169-185, 10.1016/j.jvolgeores.2009.06.012.

Freda, C., Gaeta, M., Palladino, D.M. & Trigila, R. 1997. The Villa Senni Eruption (Alban Hills, central Italy): the role of H2O and CO2 on the magma chamber evolution and on the eruptive scenario. *Journal of Volcanology and Geothermal Research*, **78**, 103-120, doi:10.1016/S0377-0273(97)00007-3.

Genareau, K., Wallace, K.L., Gharghabi, P. & Gafford, J. 2019. Lightning Effects on the Grain Size Distribution of Volcanic Ash. *Geophysical Research Letters*, **46**, 3133-3141, doi: 10.1029/2018gl081298.

Genareau, K., Wardman, J.B., Wilson, T.M., McNutt, S.R. & Izbekov, P. 2015. Lightning-induced volcanic spherules. *Geology*, **43**, 319-322, doi: 10.1130/G36255.1 %J Geology.

Genge, M.J., Davies, B., Suttle, M.D., van Ginneken, M. & Tomkins, A.G. 2017. The mineralogy and petrology of I-type cosmic spherules: Implications for their sources, origins and identification in sedimentary rocks. *Geochimica et Cosmochimica Acta*, **218**, 167-200, doi:10.1016/j.gca.2017.09.004.

Genge, M.J., Engrand, C., Gounelle, M. & Taylor, S. 2008. The classification of micrometeorites. *Meteoritics and Planetary Science*, **43**, 497-515, doi:10.1111/j.1945-5100.2008.tb00668.x

Gislason, S.R., Hassenkam, T., Nedel, S., Bovet, N., Eiriksdottir, E.S., Alfredsson, H.A., Hem, C.P., Balogh, Z.I., Dideriksen, K., Oskarsson, N., Sigfusson, B., Larsen, G. & Stipp, S.L.S. 2011. Characterization of Eyjafjallajokull volcanic ash particles and a protocol for rapid risk assessment. *Proceedings of the National Academy of Sciences of the United States of America*, **108**, 7307-7312, doi: 10.1073/pnas.1015053108.

Glass, B.P. 2016. Glass: The Geologic Connection. *International Journal of Applied Glass Science*, **7**, 435-445, doi: 10.1111/ijag.12240.

Gonnermann, H.M. & Manga, M. 2006. The Fluid Mechanics Inside a Volcano. *Annual Review of Fluid Mechanics*, **39**, 321-356, doi: 10.1146/annurev.fluid.39.050905.110207.
Graup, G. 1999. Carbonate-silicate liquid immiscibility upon impact melting: Ries Crater, Germany. *Meteoritics & Planetary Science*, **34**, 425-438, doi:10.1111/j.1945-5100.1999.tb01351.x.
Heiken, G. 1972. Morphology and Petrography of Volcanic Ashes. *GSA Bulletin*, **83**, 1961-1988, doi: 10.1130/0016-7606.
Hernando, I.R., Franzese, J.R., Llambías, E.J. & Petrinovic, I.A. 2014. Vent distribution in the Quaternary Payún Matrú Volcanic Field, western Argentina: Its relation to tectonics and crustal structures. *Tectonophysics*, **622**, 122-134, doi: 10.1016/j.tecto.2014.03.003.
Hodge, P.W. & Wright, F.W. 1964. Studies of particles for extraterrestrial origin. 2. Comparison of microscopic spherules of meteoritic and volcanic origin. *Journal of Geophysical Research*, **69**, 2449-&, doi: 10.1029/JZ069i012p02449.
Hornig-Kjarsgaard, I. 1998. Rare Earth Elements in Sövitic Carbonatites and their Mineral Phases. *Journal of Petrology*, **39**, 2105-2121, doi: 10.1093/petroj/39.11-12.2105.
Jochum, K.P., Scholz, D., Stoll, B., Weis, U., Wilson, S.A., Yang, Q., Schwalb, A., Börner, N., Jacob, D.E. & Andreae, M.O. 2012. Accurate trace element analysis of speleothems and biogenic calcium carbonates by LA-ICP-MS. *Chemical Geology*, **318-319**, 31-44, doi: 10.1016/j.chemgeo.2012.05.009.
Jones, R.E., Kirstein, L.A., Kasemann, S.A., Litvak, V.D., Poma, S., Alonso, R.N. & Hinton, R. 2016. The role of changing geodynamics in the progressive contamination of Late Cretaceous to Late Miocene arc magmas in the southern Central Andes. *Lithos*, **262**, 169-191, doi: 10.1016/j.lithos.2016.07.002.
Kay, S.M., Burns, W.M., Copeland, P. & Mancilla, O. 2006. Upper Cretaceous to Holocene magmatism and evidence for transient Miocene shallowing of the Andean subduction zone under the northern Neuquén Basin. *Special papers of the Geological Society of America*, **407**, 19-60, doi: 10.1130/20062407(02).
Kay, S.M., Jones, H.A. & Kay, R.W. 2013. Origin of Tertiary to Recent EM- and subduction-like chemical and isotopic signatures in Auca Mahuida region (37°–38°S) and other Patagonian plateau lavas. *Contributions to Mineralogy and Petrology*, **166**, 165-192, doi: 10.1007/s00410-013-0870-9.
Litvak, V.D., Poma, S., Jones, R.E., Fernández Paz, L., Iannelli, S.B., Spagnuolo, M., Kirstein, L.A., Folguera, A. & Ramos, V.A. 2018. The Late Paleogene to Neogene Volcanic Arc in the Southern Central Andes (28°–37° S). *In*: Folguera, A., Contreras-Reyes, E., Heredia, N., Encinas, A., B. Iannelli, S., Oliveros, V., M. Dávila, F., Collo, G., Giambiagi, L., Maksymowicz, A., Iglesia Llanos, M.P., Turienzo, M., Naipauer, M., Orts, D., D. Litvak, V., Alvarez, O. & Arriagada, C. (eds.) *The Evolution of the Chilean-Argentinean Andes*. Springer International Publishing, Cham, 503-536.
Liu, S., Fan, H.-R., Groves, D.I., Yang, K.-F., Yang, Z.-F. & Wang, Q.-W. 2020. Multiphase carbonatite-related magmatic and metasomatic processes in the genesis of the ore-hosting dolomite in the giant Bayan Obo REE-Nb-Fe deposit. *Lithos*, **354-355**, 105359, doi: 10.1016/j.lithos.2019.105359.
Love, S.G. & Brownlee, D.E. 1991. Heating and thermal transformation of micrometeoroids entering the Earth's atmosphere. *Icarus*, **89**, 26-43, doi: 10.1016/0019-1035(91)90085-8.
MacDonald, R., 1974. Nomenclature and petrochemistry of the peralkaline oversaturated extrusive rocks. *Bulletin Volcanologique* **38**, 498–516.

Macdonald, R., Kjarsgaard, B.A., Skilling, I.P., Davies, G.R., Hamilton, D.I. & Black, S. 1993. Liquid Immiscibility between Trachyte and Carbonate in Ash-Flow Tuffs from Kenya. *Contributions to Mineralogy and Petrology*, **114**, 276-287, doi: Doi 10.1007/Bf00307762.
Marks, M.A.W. & Markl, G. 2017. A global review on agpaitic rocks. *Earth Science Reviews* **173**, 229–258.
Martin, R., Mather, T., Pyle, D., Power, M., Allen, A., Aiuppa, A., Horwell, C. & Ward, E.J.J.o.G.R.A. 2008. Composition-resolved size distributions of volcanic aerosols in the Mt. Etna plumes. *Journal of Geophysical Research*, **113**, D17211, doi:10.1029/2007JD009648.
Martin, R.S., Mather, T.A., Pyle, D.M., Power, M., Tsanev, V.I., Oppenheimer, C., Allen, A.G., Horwell, C.J. & Ward, E.P.W. 2009. Size distributions of fine silicate and other particles in Masaya's volcanic plume. *Journal of Geophysical Research-Atmospheres*, **114**, D09217, doi:10.1029/2008JD011211.

Mather, T.A., Pyle, D.M. & Oppenheimer, C. 2003. Tropospheric Volcanic Aerosol, in Volcanism and the Earth's Atmosphere. *In*: Oppenheimer, A.R.a.C. (ed.) *Volcanism and the Earth's Atmosphere* Am. Geophys. Union,, Washington, D.C, 189-212.
Meeker, G.P. & Hinkley, T.K. 1993. The structure and composition of microspheres from the Kilauea volcano, Hawaii. *American Mineralogist*, **78,** 873-876.
Misyura, S.Y. 2017. The effect of Weber number, droplet sizes and wall roughness on crisis of droplet boiling. *Experimental Thermal and Fluid Science*, **84**, 190-198, doi: 10.1016/j.expthermflusci.2017.02.014.
Mollo, S., Giacomoni, P.P., Andronico, D. & Scarlato, P. 2015. Clinopyroxene and titanomagnetite cation redistributions at Mt. Etna volcano (Sicily, Italy): Footprints of the final solidification history of lava fountains and lava flows. *Chemical Geology*, **406**, 45-54, doi: 10.1016/j.chemgeo.2015.04.017.
Moune, S., Faure, F., Gauthier, P.-J. & Sims, K.W.W. 2007. Pele's hairs and tears: Natural probe of volcanic plume. *Journal of Volcanology and Geothermal Research*, **164**, 244-253, doi: 10.1016/j.jvolgeores.2007.05.007.
Mueller, S.B., Ayris, P.M., Wadsworth, F.B., Kueppers, U., Casas, A.S., Delmelle, P., Taddeucci, J., Jacob, M. & Dingwell, D.B. 2017. Ash aggregation enhanced by deposition and redistribution of salt on the surface of volcanic ash in eruption plumes. *Scientific Reports*, **7**, 45762, doi: 10.1038/srep45762.
Mueller, S.P., Helo, C., Keller, F., Taddeucci, J. & Castro, J.M. 2018. First experimental observations on melting and chemical modification of volcanic ash during lightning interaction. *Scientific Reports*, **8**, 1389, doi: 10.1038/s41598-018-19608-3.
Mutch, T.A. 1964. Volcanic ashes compared with Palaeozoic salts containing extraterrestrial spherules. *Journal of Geophysical Research*, **69**, 4735-4738, doi: 10.1029/JZ069i022p04735.
Obenholzner, J.H., Schroettner, H., Golob, P. & Delgado, H. 2003. Particles from the plume of Popocatépetl volcano, Mexico - The FESEM/EDS approach. *Geological Society London Special Publications*, **213**, 123-148, doi: 10.1144/GSL.SP.2003.213.01.08.
Ohtaki, K.K., Bradley, J. P. , Gillis-Davis, J.J., Taylor, G.J. & Ishii, H.A. 2019. Formation of iron-rich nanoparticles withiin glassy silicate spherules in lunar soil. *50th Lunar and Planetary Sciences Conference*.
Orgeira, M.J., Castro, L.N., Goldmann, G.A., Prezzi, C.B., Sileo, E., Vega, D.R., Franzosi, C., Acevedo, R.D., Martínez, O., Rabassa, J., Ponce, J.F. & Tófalo, O.R. 2017. Extraterrestrial microspherules from Bajada del Diablo, Chubut, Argentina. *Geoscience Frontiers*, **8**, 137-149, doi: 10.1016/j.gsf.2016.01.004.

792 Ozdemir, S., Schulz, T., Koeberl, C., Reimold, W.U., Mohr-Westheide, T., Hoehnel, D. &
793 Schmitt, R.T. 2017. Early Archean spherule layers from the Barberton Greenstone Belt,
794 South Africa: Mineralogy and geochemistry of the spherule beds in the CT3 drill core.
795 *Meteoritics & Planetary Science*, **52**, 2586-2631, doi: 10.1111/maps.12998.
796 Pallares, C., Quidelleur, X., Debreil, J.A., Antoine, C., Sarda, P., Tchilinguirian, P., Delpech, G.
797 & Gillot, P.-Y. 2019. Quaternary evolution of the El Tromen volcanic system, Argentina,
798 based on new K-Ar and geochemical data: Insights for temporal evolution of magmatic
799 processes between arc and back-arc settings. *Journal of South American Earth Sciences*, **90**,
800 338-354, doi: 10.1016/j.jsames.2018.12.022.
801 Pallares, C., Quidelleur, X., Gillot, P.-Y., Kluska, J.-M., Tchilinguirian, P. & Sarda, P. 2016. The
802 temporal evolution of back-arc magmas from the Auca Mahuida shield volcano (Payenia
803 Volcanic Province, Argentina). *Journal of Volcanology and Geothermal Research*, **323**, 19-37,
804 doi: 10.1016/j.jvolgeores.2016.04.043.
805 Pasek, M.A., Block, K. & Pasek, V. 2012. Fulgurite morphology: a classification scheme and
806 clues to formation. *Contributions to Mineralogy and Petrology*, **164**, 477-492, doi:
807 10.1007/s00410-012-0753-5.
808 Porritt, L.A., Russell, J.K. & Quane, S.L. 2012. Pele's tears and spheres: Examples from
809 Kilauea Iki. *Earth and Planetary Science Letters*, **333-334**, 171-180, doi:
810 10.1016/j.epsl.2012.03.031.
811 Preece, K., Gertisser, R., Barclay, J., Berlo, K., Herd, R.A. & Edinburgh Ion Microprobe, F.
812 2014. Pre- and syn-eruptive degassing and crystallisation processes of the 2010 and 2006
813 eruptions of Merapi volcano, Indonesia. *Contributions to Mineralogy and Petrology*, **168**,
814 1061, doi: 10.1007/s00410-014-1061-z.
815 Schaaf, P., Stimac, J.I.M., Siebe, C. & MacÍAs, J.L. 2005. Geochemical Evidence for Mantle
816 Origin and Crustal Processes in Volcanic Rocks from Popocatépetl and Surrounding
817 Monogenetic Volcanoes, Central Mexico. *Journal of Petrology*, **46**, 1243-1282, doi:
818 10.1093/petrology/egi015.
819 Schulte, P., Stinnesbeck, W., Stüben, D., Kramar, U., Berner, Z., Keller, G. & Adatte,
820 T.J.I.J.o.E.S. 2003. Fe-rich and K-rich mafic spherules from slumped and channelized
821 Chicxulub ejecta deposits in the northern La Sierrita area, NE Mexico. *International Journal*
822 *of Earth Science*, **92**, 114-142, doi: 10.1007/s00531-002-0304-9.
823 Smith, C.M., Van Eaton, A.R., Charbonnier, S., McNutt, S.R., Behnke, S.A., Thomas, R.J.,
824 Edens, H.E. & Thompson, G. 2018. Correlating the electrification of volcanic plumes with
825 ashfall textures at Sakurajima Volcano, Japan. *Earth and Planetary Science Letters*, **492**, 47-
826 58, doi: 10.1016/j.epsl.2018.03.052.
827 Søager, N., Holm, P.M. & Thirlwall, M.F. 2015. Sr, Nd, Pb and Hf isotopic constraints on
828 mantle sources and crustal contaminants in the Payenia volcanic province, Argentina. *Lithos*,
829 **212**, 368-378.
830 Spandler, C., Martin, L.H.J. & Pettke, T. 2012. Carbonate assimilation during magma
831 evolution at Nisyros (Greece), South Aegean Arc: Evidence from clinopyroxenite xenoliths.
832 *Lithos*, **146-147**, 18-33, doi: 10.1016/j.lithos.2012.04.029.
833 Sterpenich, J. & Libourel, G. 2001. Using stained glass windows to understand the durability
834 of toxic waste matrices. *Chemical Geology*, **174**, 181-193, doi: 10.1016/S0009-
835 2541(00)00315-6.
836 Suttle, M.D. & Folco, L. 2020. The Extraterrestrial Dust Flux: Size Distribution and Mass
837 Contribution Estimates Inferred From the Transantarctic Mountains (TAM) Micrometeorite

Collection. *Journal of Geophysical Research: Planets*, **125**, e2019JE006241, doi: 10.1029/2019JE006241.
Taylor, S. & Brownlee, D.E. 1991. Cosmic spherules in the geologic record. *Meteoritics*, **26**, 203-211, doi: 10.1111/j.1945-5100.1991.tb01040.x.
Veizer, J. 1983. Trace elements and isotopes in sedimentary carbonates. *Reviews in Mineralogy and Geochemistry*, **11**, 265-299.
Voldman, G.G., Genge, M.J., Albanesi, G.L., Barnes, C.R. & Ortega, G. 2013. Cosmic spherules from the Ordovician of Argentina. *Geological Journal*, **48**, 222-235, doi: 10.1002/gj.2418.
Wadsworth, F.B., Vasseur, J., Llewellin, E.W., Genareau, K., Cimarelli, C. & Dingwell, D.B. 2017. Size limits for rounding of volcanic ash particles heated by lightning. *J Geophys Res Solid Earth*, **122**, 1977-1989, doi: 10.1002/2016JB013864.
Wallace, M.W., Gostin, V.A. & Keays, R.R. 1990. Spherules and Shard-Like Clasts from the Late Proterozoic Acraman Impact Ejecta Horizon, South-Australia. *Meteoritics*, **25**, 161-165, doi: DOI 10.1111/j.1945-5100.1990.tb00991.x.
Walowski, K.J., Kirstein, L.A., De Hoog, J.C.M., Elliott, T.R., Savov, I.P. & Jones, R.E. 2019. Investigating ocean island mantle source heterogeneity with boron isotopes in melt inclusions. *Earth and Planetary Science Letters*, **508**, 97-108, doi: 10.1016/j.epsl.2018.12.005.
Wieser, P.E., Turner, S.J., Mather, T.A., Pyle, D.M., Savov, I.P. & Orozco, G. 2019. New constraints from Central Chile on the origins of enriched continental compositions in thick-crusted arc magmas. *Geochimica et Cosmochimica Acta*, **267**, 51-74, doi: 10.1016/j.gca.2019.09.008.
Wright, F.W. & Hodge, P.W. 1965. Studies of particles for extraterrestrial origin. 4. Microscopic spherules from recent volcanic eruptions. *Journal of Geophysical Research*, **70**, 3889-3898, doi: 10.1029/JZ070i016p03889.
Wright, F.W., Hodge, P.W. & Franklin, F.A. 1965. Differences between meteoritic and volcanic spherules. *Astronomical Journal*, **70**, 334-&, doi: 10.1086/109742.
Wu, Y.Z., Sharma, M., LeCompte, M.A., Demitroff, M.N. & Landis, J.D. 2013. Origin and provenance of spherules and magnetic grains at the Younger Dryas boundary. *Proceedings of the National Academy of Sciences of the United States of America*, **110**, E3557-E3566, doi: 10.1073/pnas.1304059110.

Table 1. Sample location and major element data in wt.% for tephra samples from which spherules were separated.

Sample	**NQN2**	**NQN4**	**NQN5**
Locality	Tromen	Aucun Mahuida	Aucun Mahuida
Latitude (°S)	*37.023*	*37.535*	*37.597*
Longitude (°W)	*69.851*	*68.695*	*68.560*
SiO_2	48.94	45.29	47.19
TiO_2	1.59	2.08	1.89
Al_2O_3	16.63	13.57	14.53
Fe_2O_3	11.13	12.02	11.64
MnO	0.17	0.16	0.16
MgO	6.23	9.98	9.13
CaO	10.19	9.83	9.56
Na_2O	3.23	2.07	2.27
K_2O	0.77	0.98	1.02
P_2O_5	0.23	0.57	0.42
LOI	0.47	3.22	2.46
Total	99.57	99.76	100.27

*LOI – loss on ignition

Table 2. Major element composition of a variety of spherules/spheroids from the samples analysed. Both core and rims were analysed for each particle. Number in parenthesis is the number of individual analyses that have been averaged for these composition totals, full dataset available in Supplementary file A.

Spherule composition

(wt.%)	SiO_2	TiO_2	Al_2O_3	MgO	CaO	FeO	Na_2O	K_2O	MnO	P_2O_5	SO_2	F	Cl	Total
NQN2 F Core (4)	73.52	0.03	1.15	0.12	12.21	0.08	13.67	0.40	0.03	0.02	0.26	0.00	0.02	100.95
±	*0.91*	*0.00*	*0.09*	*0.01*	*0.10*	*0.04*	*0.08*	*0.03*	*0.01*	*0.01*	*0.01*		*0.00*	
NQN2 F Rim (4)	73.15	0.03	1.11	0.10	12.01	0.06	12.94	0.40	0.03	0.01	0.26	0.03	0.02	100.09
±	*1.57*	*0.00*	*0.07*	*0.02*	*0.19*	*0.05*	*1.47*	*0.04*	*0.00*	*0.01*	*0.01*		*0.00*	
NQN2 II Core (7)	75.02	*nm*	1.76	0.01	6.72	0.06	16.15	0.28	0.01	0.04	0.32	0.49	0.23	100.86
±	*0.35*		*0.12*	*0.02*	*0.16*	*0.02*	*0.23*	*0.02*	*0.01*	*0.01*	*0.01*	*0.02*	*0.00*	
NQN2 II Rim (6)	73.81	*nm*	1.72	0.00	6.65	0.04	15.87	0.27	0.01	0.04	0.31	0.42	0.23	99.16
±	*0.76*		*0.14*	*0.00*	*0.15*	*0.02*	*0.29*	*0.03*	*0.01*	*0.01*	*0.01*	*0.05*	*0.00*	
NQN2 A Core (9)	72.88	0.03	1.05	0.17	11.61	0.15	14.20	0.37	0.03	0.02	0.22	0.00	0.02	100.75
±	*0.55*	*0.00*	*0.09*	*0.01*	*0.12*	*0.07*	*0.20*	*0.05*	*0.01*	*0.01*	*0.01*	*0.01*	*0.00*	
NQN2 A Rim (3)	72.25	0.03	1.13	0.20	11.75	0.23	14.14	0.39	0.03	0.02	0.21	0.01	0.02	100.41
±	*0.12*	*0.00*	*0.07*	*0.05*	*0.19*	*0.11*	*0.37*	*0.06*	*0.01*	*0.00*	*0.01*	*0.01*	*0.00*	
NQN2 B Core (4)	72.06	0.10	0.65	3.64	9.18	0.13	14.06	0.18	0.00	0.00	0.22	0.00	0.01	100.25
±	*0.45*	*0.00*	*0.08*	*0.07*	*0.17*	*0.05*	*0.11*	*0.04*	*0.00*	*0.00*	*0.00*	*0.00*	*0.00*	
NQN2 B Rim (2)	71.76	0.10	0.72	3.71	9.07	0.11	13.79	0.19	0.00	0.01	0.24	0.00	0.01	99.69
±	*0.19*	*0.00*	*0.04*	*0.03*	*0.03*	*0.15*	*0.20*	*0.01*	*0.00*	*0.01*	*0.01*	*0.00*	*0.00*	
NQN2 C Core (7)	73.20	0.02	0.14	3.61	9.40	0.09	13.61	0.01	0.01	0.01	0.19	0.00	0.01	100.29
±	*0.62*	*0.00*	*0.05*	*0.10*	*0.16*	*0.03*	*0.21*	*0.01*	*0.01*	*0.00*	*0.01*	*0.00*	*0.00*	
NQN2 E Core (4)	73.54	0.03	0.31	3.86	8.63	0.52	13.57	0.16	0.01	0.01	0.19	0.00	0.02	100.84
±	*0.54*	*0.00*	*0.07*	*0.06*	*0.12*	*0.07*	*0.22*	*0.04*	*0.01*	*0.00*	*0.01*	*0.00*	*0.00*	
NQN4 II B Core (2)	48.93	3.19	15.23	4.38	9.64	11.84	3.94	1.97	0.17	0.88	0.06	0.13	0.04	100.38
±	*0.23*	*0.00*	*0.54*	*0.11*	*0.05*	*0.18*	*0.15*	*0.01*	*0.00*	*0.00*	*0.00*	*0.01*	*0.00*	
NQN4 II B Rim (1)	49.33	3.24	15.20	4.37	9.71	11.90	3.26	1.93	0.16	0.89	0.06	0.10	0.04	100.17
NQN4 II C Core (3)	39.77	0.03	0.10	40.28	0.31	19.19	0.02	0.01	0.24	0.06	0.01	*nm*	0.00	99.88
±	*0.41*	*0.01*		*0.13*	*0.05*	*0.33*	*0.00*	*0.01*	*0.01*	*0.01*	*0.00*		*0.00*	

NQN4 II C Rim (1)	48.65	3.21	15.91	4.28	9.78	11.49	3.57	1.92	0.17	0.89	0.07	0.12	0.04	100.11
NQN4 A Core (3)	0.02	12.53	3.49	3.58	0.03	74.67	0.02	0.02	0.55	0.00	0.00	0.02	0.00	94.90
±	*0.02*	*0.01*	*0.13*	*0.16*	*0.01*	*1.84*	*0.01*	*0.01*	*0.00*	*0.00*	*0.00*	*0.01*	*0.00*	
NQN4 A Rim (3)	0.05	12.50	3.49	3.65	0.02	75.99	0.09	*nd*	0.55	0.01	0.01	0.02	0.00	96.25
±	*0.03*	*0.05*	*0.30*	*0.08*	*0.02*	*0.33*			*0.00*	*0.00*	*0.00*	*0.00*	*0.00*	
NQN5 B Core (4)	0.04	0.00	0.05	0.06	55.67	0.09	0.00	0.04	0.02	0.02	0.03	0.04	0.00	55.95
±	*0.03*	*0.00*	*0.05*	*0.03*	*0.11*	*0.08*	*0.00*	*0.04*	*0.01*	*0.01*	*0.03*	*0.02*	*0.00*	
NQN5 B Rim (2)	0.04	*nm*	0.04	0.10	55.40	0.02	0.01	0.01	0.01	0.04	0.12	0.07	0.01	55.87
±	*0.04*		*0.06*	*0.01*	*0.28*	*0.02*		*0.00*	*0.00*	*0.00*	*0.03*	*0.01*	*0.00*	
NQN5 C Core (3)	0.05	0.00	0.08	0.18	55.05	0.07	0.05	0.03	0.01	0.08	0.37	0.15	0.00	55.89
±	*0.04*			*0.08*	*1.20*	*0.00*	*0.06*		*0.00*	*0.06*	*0.25*	*0.00*	*0.00*	
NQN5 C Rim (3)	0.04	0.00	0.07	0.13	54.95	0.13	0.05	0.02	0.01	0.13	0.53	0.15	0.01	56.09
±	*0.03*		*0.02*	*0.04*	*0.03*	*0.06*	*0.02*	*0.00*	*0.00*	*0.02*	*0.01*	*0.02*	*0.00*	
NQN4 II E Core (4)	0.02	0.00	0.05	0.10	56.84	0.03	0.03	0.02	0.00	0.07	0.01	0.03	0.00	57.07
±	*0.01*	*0.00*	*0.05*	*0.02*	*0.24*	*0.03*		*0.01*	*0.00*	*0.04*	*0.01*	*0.03*	*0.00*	
NQN4 II E Rim (4)	0.03	0.00	0.01	0.22	55.90	0.09	0.02	0.01	0.01	0.06	0.01	0.05	0.01	56.21
±	*0.03*	*0.00*	*0.00*	*0.05*	*1.01*	*0.01*	*0.02*	*0.01*	*0.01*	*0.08*	*0.01*	*0.04*	*0.00*	

nm – not measured.

Table 3. Selected trace element composition of carbonate spheroids from sample NQN5 compared with published data from Liu et al. (2020)* and Jochum et al. (2012)^. 05B157 – calcite grains in Ca-carbonatite dyke; 06B272 – calcite from limestone; S1^ - stalagmite representing meteoric component.

	NQN5	NQN5 A	NQN5 C1	NQN5 $C3_{rim}$	05B157*	06B272*	S1^
Sr	611.3	380.9	512.1	202.4	6379	193	52.0
Y	19.8	0.56	2.32	0.06	41.0	14.5	0.23
Ba	235.7	6.75	7.62	4.20	64.4	13.9	5.6
La	18.03	0.61	4.39	0.05	2.2	6.2	0.11
Ce	38.88	0.08	0.14	0.05	6.7	9.0	0.19

Figure 1.

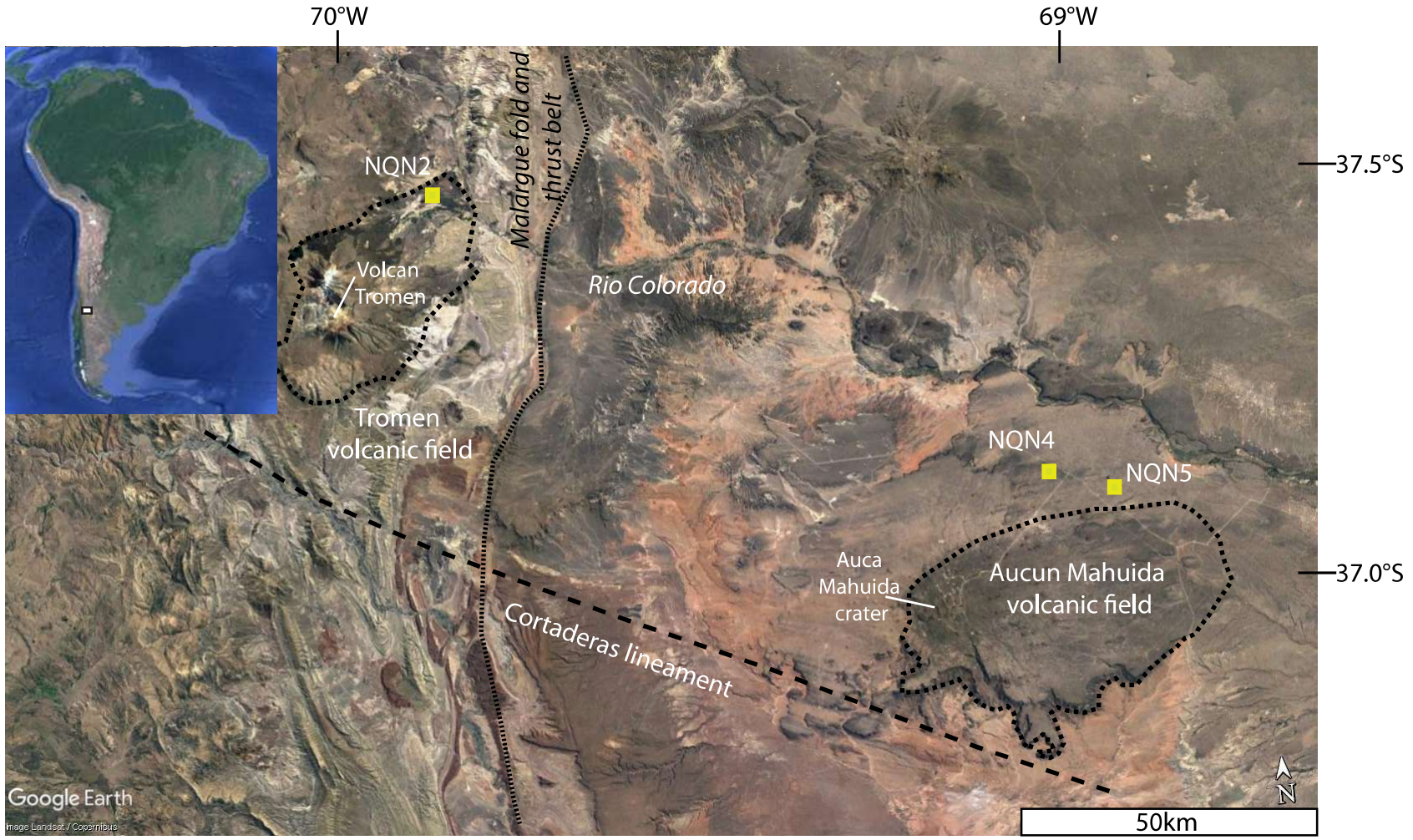

Figure 2.

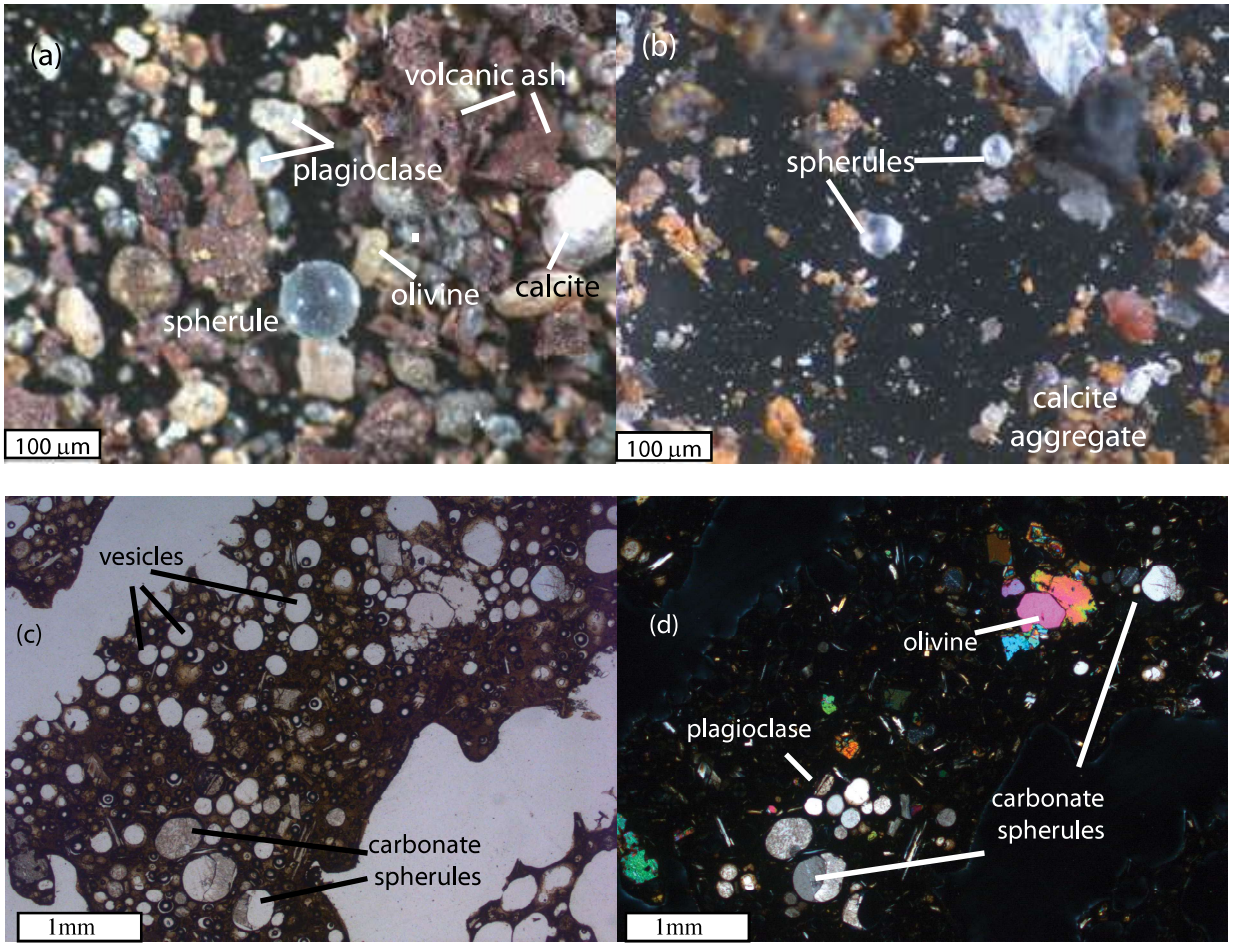

figure 3

Click here to access/download;figure;Figure 3_annotated.pdf

Figure 3.

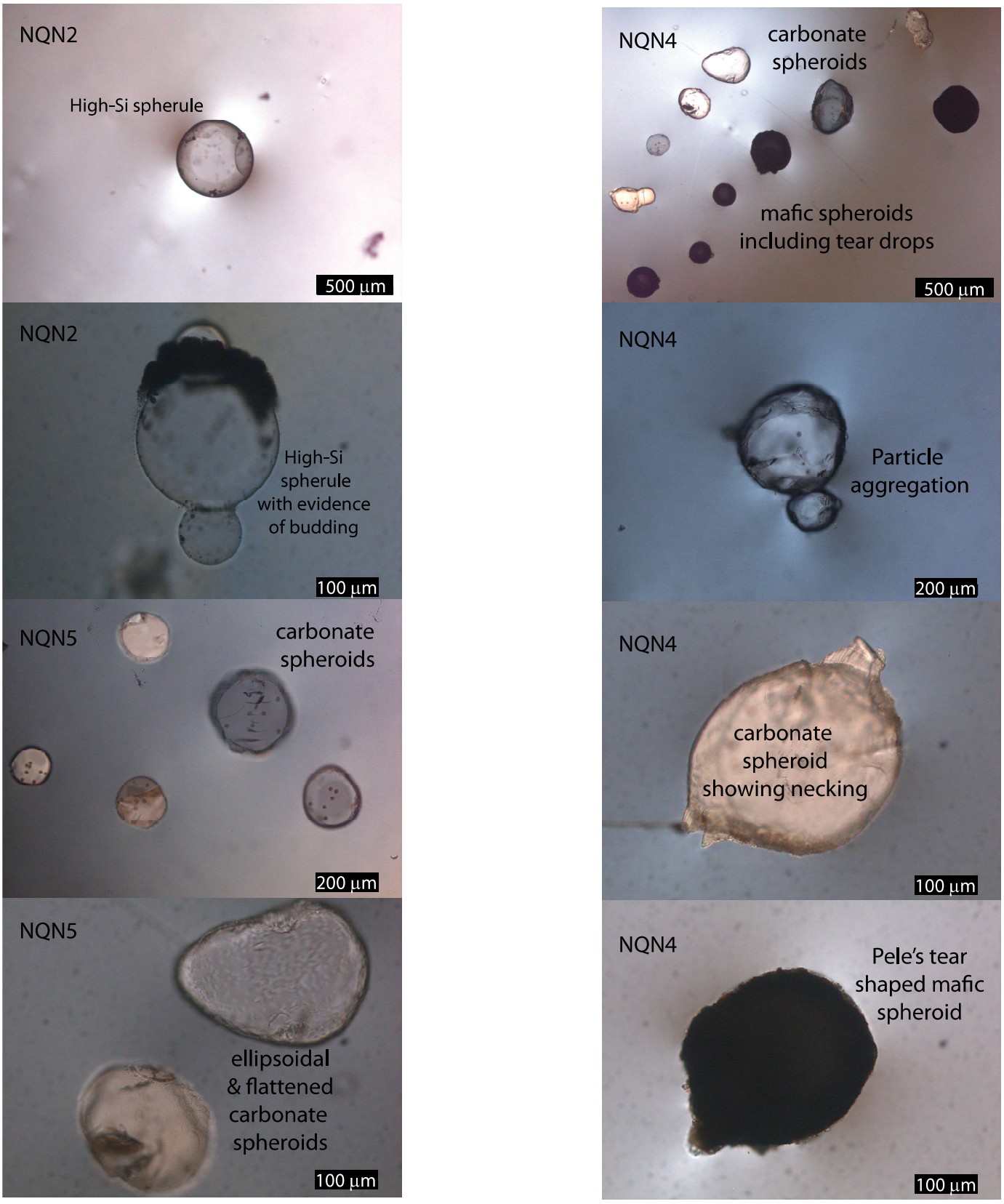

Figure 4.

(a)

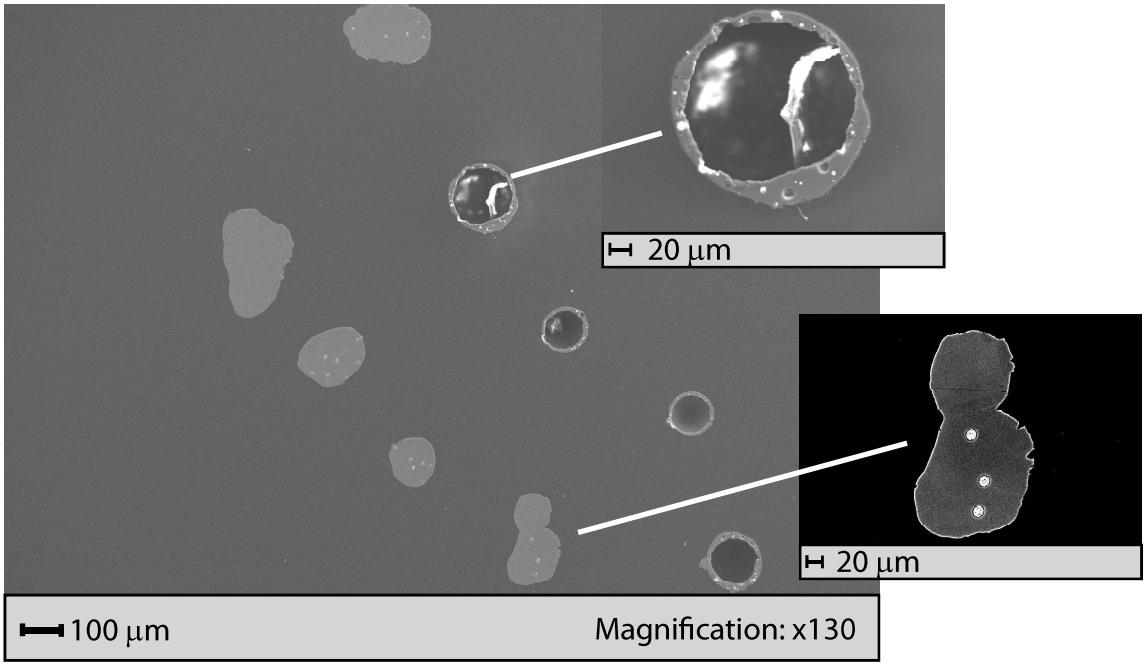

(b)

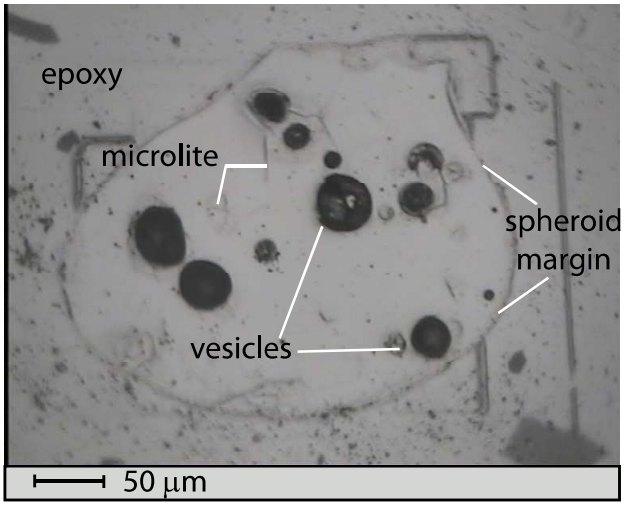

Figure 5.

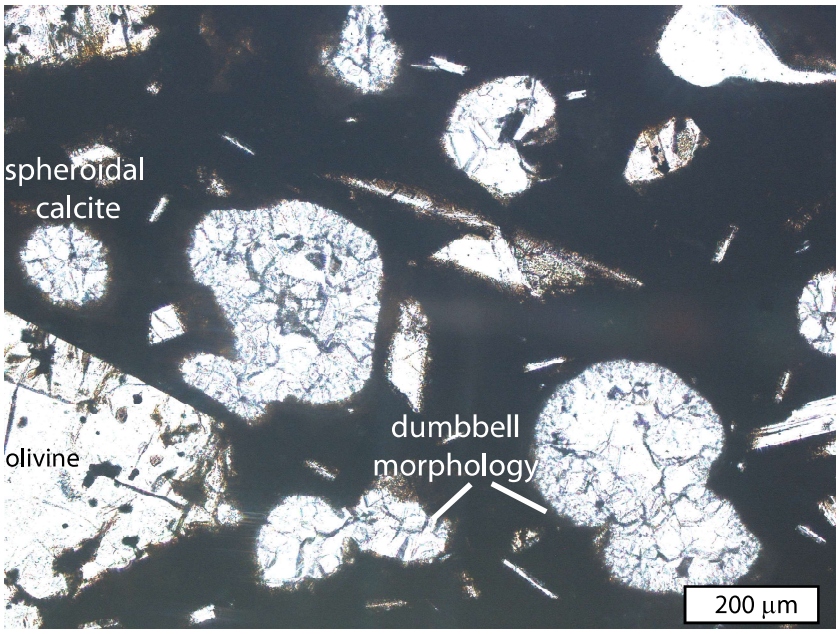

figure 6

Click here to access/download;figure;Figure 6_new.pdf

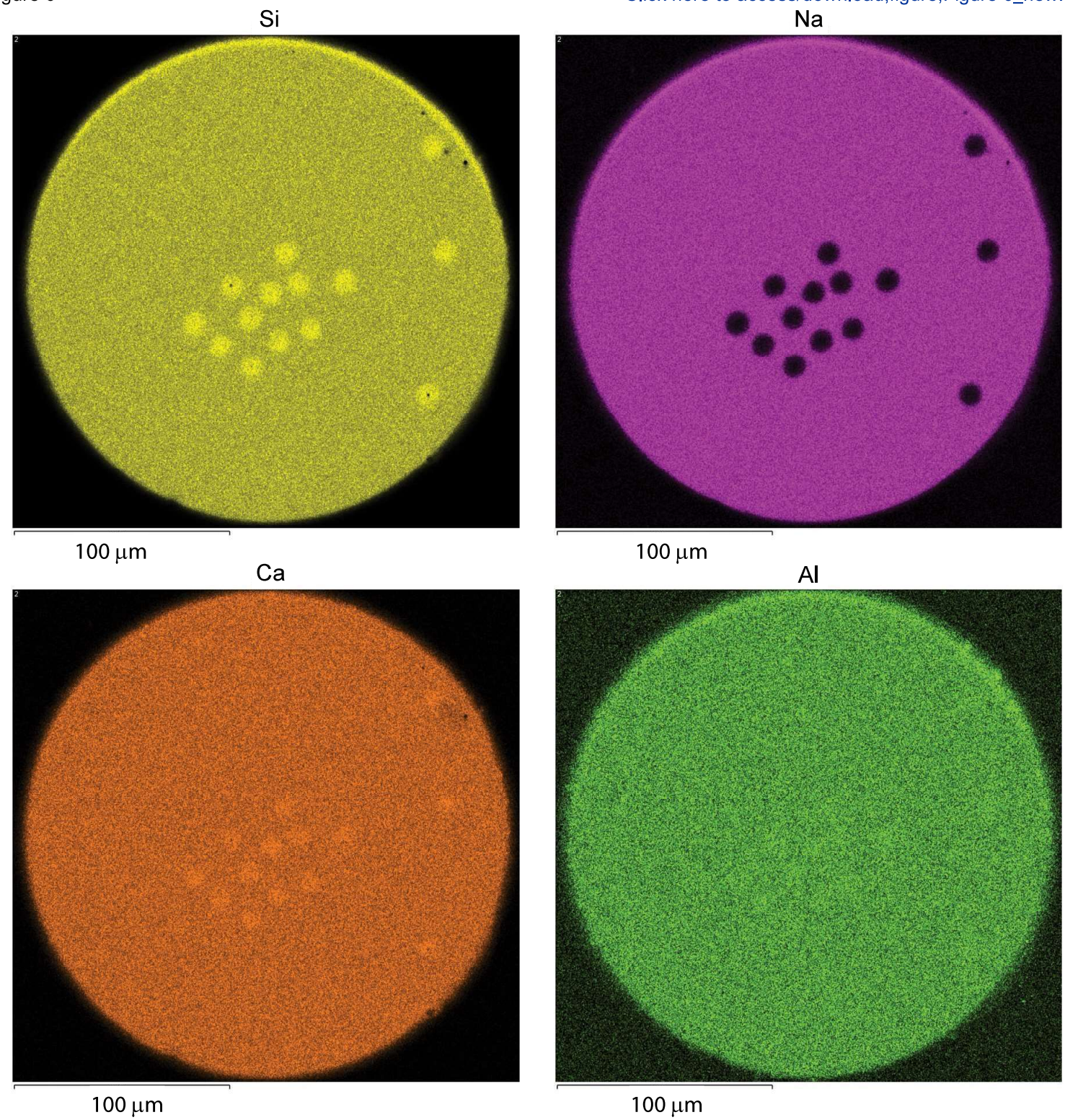

Figure 6.

Figure 7a.

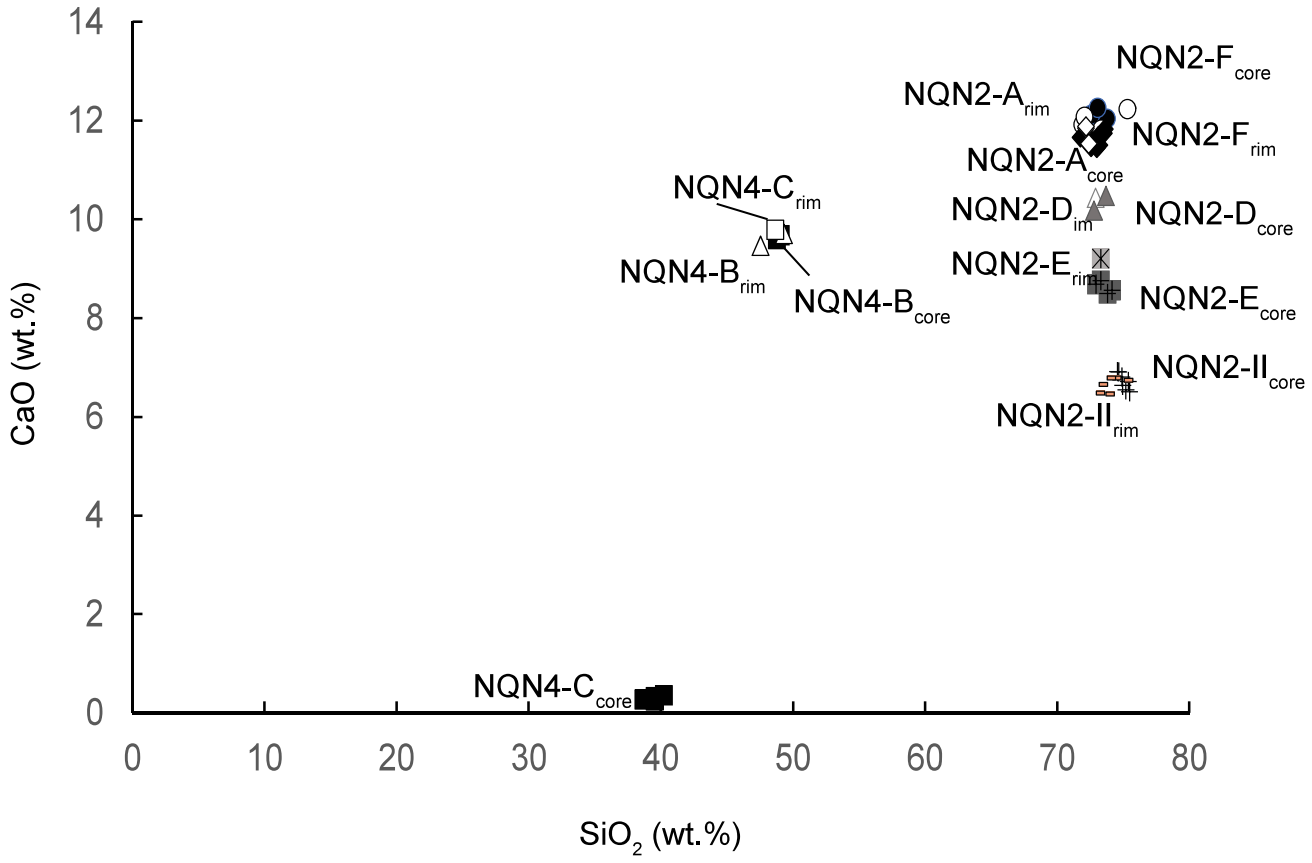

Figure 7b.

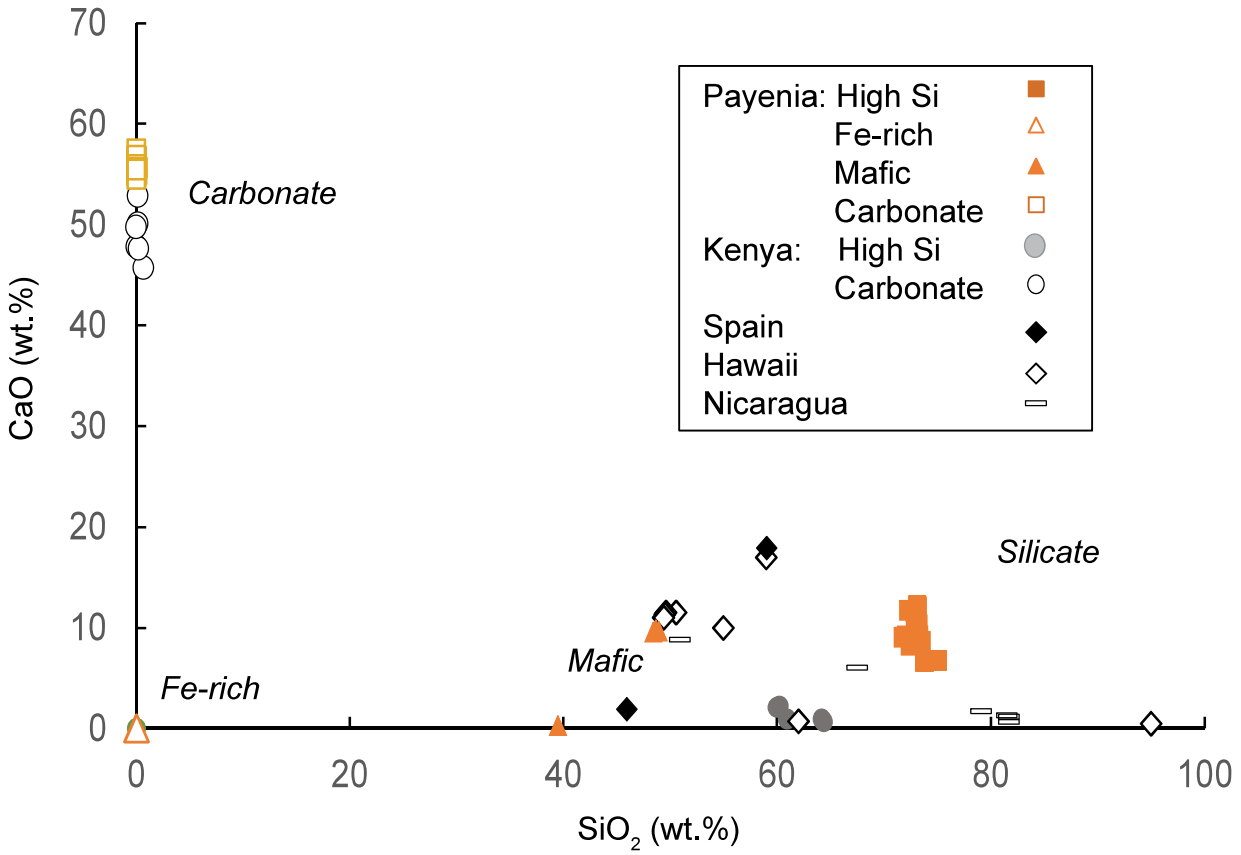

Figure 8.

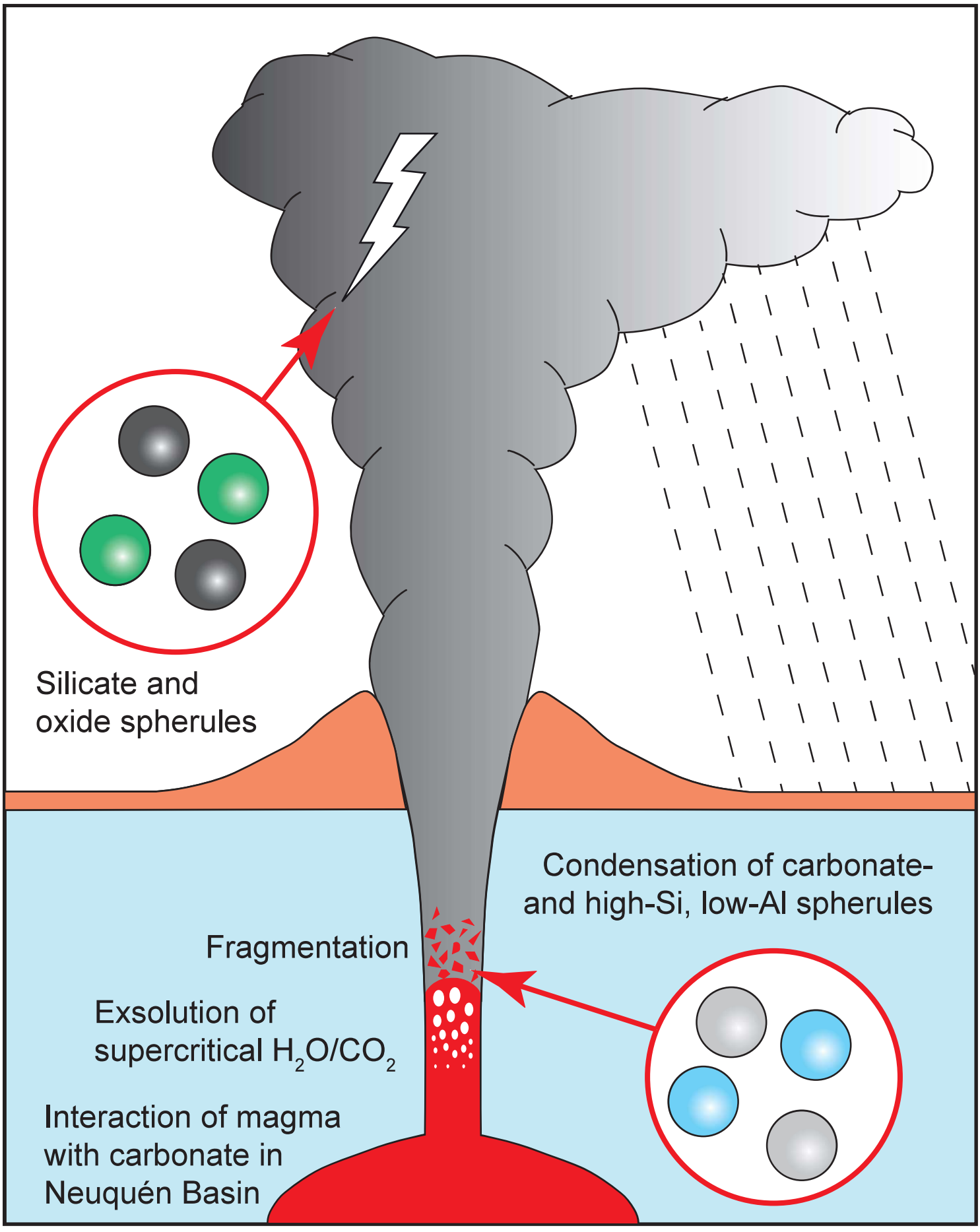

Click here to access/download
supplementary material
Supplementary file A_ data_all.xlsx